JOURNAL OF GEOPHYSICAL RESEARCH, VOL. 113, E11004, doi:10.1029/2008JE003160, 2008

Photochemical instability of the ancient Martian atmosphere

Kevin Zahnle,[1] Robert M. Haberle,[1] David C. Catling,[2] and James F. Kasting[3]

Received 2 April 2008; accepted 29 July 2008; published 6 November 2008.

[1] We develop a 1-D steady state photochemical model of the modern Martian atmosphere and apply it to possible Martian atmospheres present and past. A unique feature of our model is that the major current sink of oxygen is dry deposition (surface reactions) of highly reactive, oxidized molecules (chiefly H_2O_2), rather than oxygen escape to space. Another difference is that we allow hydrogen to escape to space at the diffusion limit, which gives H escape fluxes ~70% higher than in other models. What results is a model with one free parameter: a dry deposition velocity to describe the surface sink of reactive molecules. An effective global average deposition velocity of 0.02 cm s^{-1} for H_2O_2 and O_3 gives a good match to the observed abundances of O_2, CO, and H_2, the three abundant photochemical trace gases. We then apply our model to Martian atmospheres with different amounts of CO_2, H_2O, and solar forcing. We find that thick, cold, dry CO_2 atmospheres are photochemically unstable with respect to conversion to CO. This may be pertinent to ancient Mars when the Sun was faint and O escape rates were likely high, for which the tipping point is computed to be ~10 mbar of CO_2. The possible photochemical instability of cold thick CO_2 atmospheres, and the high likelihood that CO was abundant even if CO_2 were stable, has broad implications for early Mars.

Citation: Zahnle, K., R. M. Haberle, D. C. Catling, and J. F. Kasting (2008), Photochemical instability of the ancient Martian atmosphere, *J. Geophys. Res.*, *113*, E11004, doi:10.1029/2008JE003160.

1. Introduction

[2] To first approximation the Martian atmosphere is composed of CO_2 and H_2O and their photochemical byproducts [*McElroy and Donahue*, 1972; *Yung and DeMore*, 1998]. The major products are CO, O_2, and H_2; minor ones include H_2O_2 and O_3. None of these are expected to have significant sources apart from photochemistry. Measured abundances of O_2, CO, and H_2 are reported to be 1200–2000 ppm, 800 ppm, and 17 ppm, respectively [*Krasnopolsky*, 2006]. From the dispersion seen in published estimates, the uncertainties in these abundances appear to be at least 30%. Figure 1 gives a schematic overview of Martian atmospheric photochemistry.

[3] The Martian atmosphere today is rather strongly oxidized. If there were no sinks on the photochemical products, the abundances of O_2, CO, and H_2 would sum to redox neutrality. It is convenient to define CO_2, H_2O, and N_2 as redox neutral [*Kasting and Brown*, 1998]. We can then approximate the net redox imbalance of the atmosphere by $p\mathrm{Ox} \equiv 2p\mathrm{O}_2 - p\mathrm{CO} - p\mathrm{H}_2$. In a redox neutral atmosphere pOx = 0. On Mars today $p\mathrm{Ox} \approx 10 - 15$ μbar. bar. This superabundance of O_2 represents a net buildup of oxygen generated by hydrogen escape to space. The source of the hydrogen is photolytic destruction of water vapor. On the basis of atomic hydrogen densities retrieved by fitting Mariner 6 and 7 Lyα scattering data [*Anderson and Hord*, 1971], the current H escape flux has been widely taken to be $\sim 2.4 \times 10^8$ molecules cm^{-2} s^{-1} [e.g., *Nair et al.*, 1994; *Krasnopolsky*, 1995, 2006]. At this rate it takes 10^5 years to build up the observed pOx, which is comparable to the timescale for obliquity variations. The oxidation timescale is therefore long enough that we should not, in general, expect the oxidation state of the Martian atmosphere to be in steady state with its boundary conditions, although we do expect the composition of the atmosphere to be in steady state with the current oxidation state (i.e., the O_2, CO, and H_2 abundances should be in equilibrium with pOx, but pOx itself need not be in steady state). With this caveat made, we will restrict our scope in this paper to steady state models.

[4] In steady state, oxygen sinks balance hydrogen loss to space (Figure 1). One widely discussed possibility is that oxygen also escapes to space at half the rate that H escapes, so that on net H_2O escapes [*McElroy*, 1972; *Liu and Donahue*, 1976; *McElroy et al.*, 1977]. For example, *McElroy* [1972] showed that oxygen can escape to space from Mars after dissociative recombination of O_2^+ ions. The early studies pointed out that oxygen in the atmosphere is self-regulating, with H_2 formation and therefore hydrogen escape suppressed by the buildup of O_2, a result that remains generally true. Most steady state photochemical models have imposed a fixed O escape flux at the upper boundary to balance H escape [e.g., *Krasnopolsky*, 1993,

[1]NASA Ames Research Center, Moffett Field, California, USA.
[2]Department of Earth Sciences, University of Bristol, Bristol, UK.
[3]Department of Geosciences, Pennsylvania State University, State College, Pennsylvania, USA.

0148-0227/08/2008JE003160$09.00

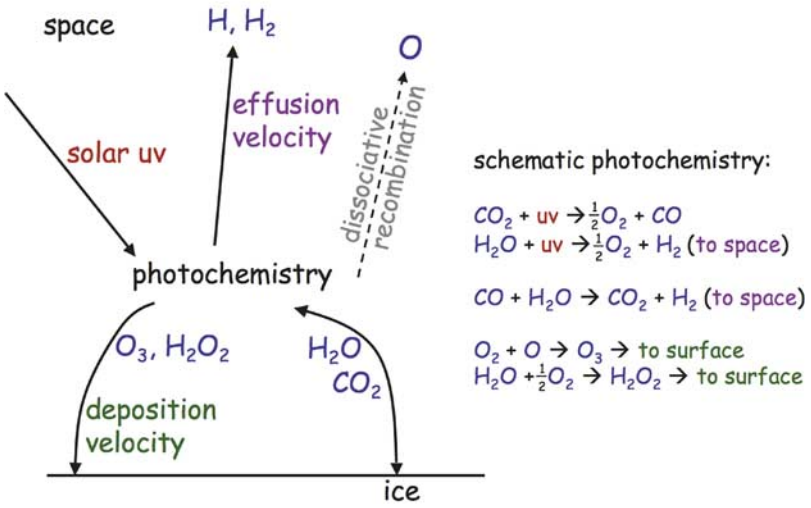

Figure 1. Schematic overview of Martian atmospheric photochemistry. Solar UV splits CO_2 and H_2O into O_2, CO, H_2, and other species. Hydrogen escape can be described by an effusion velocity v_{eff} that is less than or equal to the diffusion-limited velocity v_{lim}. The surface sink on highly oxidized species (e.g., H_2O_2 and O_3) is described by a deposition velocity v_{dep}. In steady state the net oxidation state of the atmosphere is determined by the ratio of v_{eff} and v_{dep}. Oxygen escape to space is apparently negligible at present [*Lammer et al.*, 2003] but is included in our models of ancient atmospheres, for which it is likely to be important.

1995; *Nair et al.*, 1994; *Wong et al.*, 2003]. However, a long list of spacecraft measurements and theoretical calculations presents a clear consensus that the O escape rate is of the order of 1×10^7 atoms cm^{-2} s^{-1} or less, which is more than an order of magnitude short of what is needed to maintain redox balance [*Fox and Hac*, 1997; *Lammer et al.*, 2003].

[5] An alternative oxygen sink is reaction of oxidized gases with reduced minerals in the soil to make sulfates and ferric iron [*Huguenin*, 1973, 1976; *McElroy and Kong*, 1976; *McElroy et al.*, 1977; *Hunten*, 1979; *Bullock et al.*, 1994; *Lammer et al.*, 2003]. Martian soils have long been known to be strongly oxidized, beginning from the simple observation that Mars is red, through the curious results obtained by the Viking biology experiments [*Biemann et al.*, 1977; *Klein*, 1977; *Oyama and Berdahl*, 1979], to the famous adventures of the Mars Exploration Rovers [*Squyres and Knoll*, 2005]. Hydrogen escape is the only known process capable of oxidizing Mars, and therefore atmospheric gases are the only plausible oxidizing agents for the soils. This is a conclusion strongly and independently supported by the anomalous mass fractionations seen in the oxygen and sulfur isotopes in the SNC meteorites, distinctive fractionations that demand an atmospheric photochemical source [*Farquhar et al.*, 2000, 2007]. *Nair et al.* [1994] showed that to first approximation, a photochemical code tuned to modern Mars is indifferent to whether oxygen is removed from the top or from the bottom of the atmosphere. In their numerical experiment, they removed O_2 at the ground at a fixed flux. This is essentially what *Huguenin* [1976] proposed (photostimulated by UV), and what *McElroy and Kong* [1976] addressed.

[6] We agree with *Lammer et al.* [2003] that the redox budget today has to be balanced by a surface sink on oxygen. In most of our models we treat the oxygen sink as a dry deposition velocity, v_{dep}, on highly reactive oxidized species, the most important of which are hydrogen peroxide (H_2O_2) and ozone (O_3). ("Wet deposition" implies rainout, which is not currently a major process on Mars.) Hydrogen peroxide has been a popular candidate as a soil oxidant because it is produced by atmospheric photochemistry [*Hunten*, 1979] and it provides a good fit to the results of the Viking labeled release experiment [*Oyama and Berdahl*, 1979]. In section 5.4 we consider the effect of balancing the redox budget by applying a deposition velocity to O_2 itself (i.e., models in which O_2 gas is the chief oxidizing agent).

[7] A deposition velocity sweeps all the complexities of atmospheric mixing to the surface, sticking, and reacting with the surface (chemical composition, topography, etc) into a single parameter [*Seinfeld and Pandis*, 2006]. On Earth, v_{dep} differs greatly between species; it is often highest when the surface is wet and the species soluble. Dry deposition is usually pictured as three resistances in series, one imposed by mixing through the lower atmosphere, one by molecular diffusion through the very thin laminar layer in contact with the surface, and the third by what happens when the molecule actually strikes the surface [*Seinfeld and Pandis*, 2006]. The two atmospheric transport terms are not independent, because the thickness of the thin laminar boundary layer is in part determined by atmospheric turbulence. The lower Martian atmosphere is both thinner and more turbulent than Earth's. This means that both atmospheric transport terms are faster on Mars than on Earth. Hence the bottleneck on Mars is almost certainly uptake by the surface. The generally dry, oxidized surface suggests that dry deposition velocities of water soluble or highly oxidized species are not likely to be very high on Mars, but we will find that they do not have to be high; indeed, we

will find that they cannot be high. As a first approximation we assume that the same dry deposition velocity applies to all reactive species.

[8] In this paper, we first describe the photochemical model. This is followed by a discussion of the key boundary conditions, especially hydrogen escape. The model is applied and tuned to current Mars. We then consider how the model responds to changing amounts of CO_2 and H_2O, and how it responds to higher levels of solar UV and to significant rates of O escape driven by a much more vigorous ancient solar wind. This leads into a discussion of the photochemical stability of the CO_2 atmosphere.

2. General Code Features

[9] There are many published steady state 1-D photochemical models of the Martian atmosphere [*McElroy and Donahue*, 1972; *Liu and Donahue*, 1976; *McElroy et al.*, 1977; *Krasnopolsky*, 1993, 1995, 2006; *Nair et al.*, 1994; *Atreya and Gu*, 1994; *Wong et al.*, 2003]. These codes resemble each other in their fundamental structure; our code, which is based on the photochemistry model for early Earth described by *Kasting et al.* [1989] and *Kasting* [1990], is similar. The version used here was developed from the 1989 version; many of its features are described by *Kasting et al.* [1989] and *Kasting* [1990]. We have successfully used the new code to study sulfur photochemistry of Earth's atmosphere during the Archean [*Zahnle et al.*, 2006; *Claire et al.*, 2006].

[10] Our model uses a uniform 1 km resolution grid and time marches to a steady state using the reverse Euler method. Vertical transport occurs by eddy transport and, for H and H_2, molecular diffusion. For Mars we have described eddy transport by $K = 10^6$ cm^2 s^{-1} for $z < 20$ km and $K = 10^6 \sqrt{N(z)/N(20\text{ km})}$ cm^2 s^{-1} for $20 < z < 110$ km. The surface pressure is 6.3 mbar, and the composition is 95% CO_2. The temperature profile is $T = T_0 - 1.4z$ for $z <$ 50 km and isothermal above. In our standard model, $T_0 =$ 211 K. The model is insensitive to temperature save for the effect temperature has on absolute humidity. For water vapor we use a fixed 17% relative humidity near the surface to give 9.5 precipitable microns of water. Lower temperatures aloft cause the relative humidity to rise with altitude, and water can condense. In our nominal models the global average relative humidity in the stratosphere is typically ~60%, but there is some variation because of the way water condensation has been implemented.

[11] Chemical species, reactions, and photolysis channels important to C-H-O Martian photochemistry in the modern atmosphere are listed in Table 1. Where possible the reaction rates are those recommended by *Sander et al.* [2003], or updated reaction rates taken from the online NIST database (http://kinetics.nist.gov). The list was current as of November 2007. Table 1 lists the specific sources for the specific reaction rates taken from the NIST database. Of course, some reactions are very poorly known and some are not known at all. Usually the model is insensitive to poorly known reaction rates, because these are usually not very important reactions. But there are exceptions to this generalization. We give two examples of sensitive reactions that we found through error and trial. The reaction between H and HO_2 has three reported channels. The H_2 abundance predicted by the model is sensitive to the branching ratio for forming H_2 and O_2. According to *Sander et al.* [2003], different experiments have reported this branching ratio as 0.08 ± 0.04, 0.09 ± 0.045, and 0.29 (no error given). This wide range of possibilities generates a wide range of outcomes, as this is one of the chief reactions making H_2. Low values of this branching ratio produce generally better fits to Mars. We use 0.08 in our models.

[12] A second example of an uncertain reaction is the three-body formation of the formyl radical (HCO): H + CO + M → HCO + M, where M is CO_2. The uncertainty here is in the temperature dependence of the reaction. According to most reports this should be a slow reaction at Martian temperatures, but there is at least one study that gives this reaction a relatively small activation energy [*Wagner and Bowman*, 1987], so that it would dominate the H_2 formation rate under Martian conditions. We found that when using the Wagner and Bowman rate, we inevitably predicted H_2 mixing ratios greater than 100 ppm, far in excess of what is present on Mars. We conclude that a high rate of HCO formation at low temperatures is inappropriate. We have adopted the intermediate temperature dependence recommended by *Baulch et al.* [1994], which makes the reaction generally unimportant. Consequently formaldehyde is not an important photochemical product in the models reported here.

[13] For completeness we have included nitrogen photochemistry. Species and reactions used in the code are listed in Table 2. Upper boundary conditions are inflows of 2×10^6 cm^{-2} s^{-1} for N and 2×10^7 cm^{-2} s^{-1} for NO. These are created by ionospheric chemistry which is not included in this model. The magnitudes of the N and NO fluxes are consistent with those used by *Krasnopolsky* [1995]. Redox balance is maintained by imposing an upper inflow boundary flux of 2×10^7 cm^{-2} s^{-1} on CO. These influxes are implicitly balanced by upward flows of N_2 and CO_2. Overall, the influence of nitrogen photochemistry on the C-H-O system appears to be relatively small, and we will not discuss it further here.

3. Boundary Conditions

[14] A steady state model of the current Martian atmosphere's redox state can be described by two free parameters, one of which controls hydrogen escape and the other controls oxygen loss. In our models, the two parameters are the hydrogen effusion velocity v_{eff} and the deposition velocity v_{dep} of highly reactive species, respectively. Here we discuss how we pick these two parameters.

3.1. Hydrogen Escape

[15] A feature of our code is that we truncate the vertical extent of the atmosphere at 110 km. We do not attempt to construct an ionosphere, a thermosphere, or an exosphere, and we do not attempt to explicitly compute hydrogen escape. Instead we use a hydrogen effusion velocity v_{eff} to describe how quickly hydrogen escapes from the top of the model. We express v_{eff} as a fraction of the diffusion-limited effusion velocity v_{lim}. Advantages of our approach are simplicity and clarity: our discussion of hydrogen escape is presented directly in terms of a firm physical upper limit. Moreover, as we shall argue below, the actual rate of H

Table 1. Basic H, C, O Reactions

Reactants	Products	Reaction Rate[a]	Reference[b]
$H_2O + O(^1D)$	$\rightarrow OH + OH$	2.2×10^{-10}	*Sander et al.* [2003]
$H_2 + O(^1D)$	$\rightarrow OH + H$	1.1×10^{-10}	*Sander et al.* [2003]
$H_2 + O$	$\rightarrow OH + H$	$1.34 \times 10^{-15} (T/298)^{6.52} e^{-1460/T}$	*Robie et al.* [1990]
$H_2 + OH$	$\rightarrow H_2O + H$	$5.5 \times 10^{-12} e^{-2000/T}$	*Sander et al.* [2003]
$H + O_3$	$\rightarrow OH + O_2$	$1.4 \times 10^{-10} e^{-470/T}$	*Sander et al.* [2003]
$H + O_2 + M$	$\rightarrow HO_2 + M$	7.5×10^{-11} [c]	*Sander et al.* [2003]
		$1.4 \times 10^{-31} (300/T)^{1.6}$ [d,e]	*Sander et al.* [2003]
$H + HO_2$	$\rightarrow H_2 + O_2$	$0.08 \times 8.0 \times 10^{-11}$ [f]	*Sander et al.* [2003]
$H + HO_2$	$\rightarrow H_2O + O$	$0.02 \times 8.0 \times 10^{-11}$	*Sander et al.* [2003]
$H + HO_2$	$\rightarrow OH + OH$	$0.90 \times 8.0 \times 10^{-11}$	*Sander et al.* [2003]
$OH + O$	$\rightarrow H + O_2$	$2.2 \times 10^{-11} e^{120/T}$	*Sander et al.* [2003]
$OH + HO_2$	$\rightarrow H_2O + O_2$	$4.8 \times 10^{-11} e^{250/T}$	*Sander et al.* [2003]
$OH + O_3$	$\rightarrow HO_2 + O_2$	$1.7 \times 10^{-12} e^{-940/T}$	*Sander et al.* [2003]
$HO_2 + O$	$\rightarrow OH + O_2$	$3.0 \times 10^{-11} e^{200/T}$	*Sander et al.* [2003]
$HO_2 + O_3$	$\rightarrow OH + 2O_2$	$1.0 \times 10^{-14} e^{-490/T}$	*Sander et al.* [2003]
$HO_2 + HO_2$	$\rightarrow H_2O_2 + O_2$	$2.3 \times 10^{-13} e^{600/T}$ [c]	*Sander et al.* [2003]
		$4.3 \times 10^{-33} e^{1000/T}$ [d,e]	*Sander et al.* [2003]
$H_2O_2 + OH$	$\rightarrow HO_2 + H_2O$	$2.9 \times 10^{-12} e^{-160/T}$	*Sander et al.* [2003]
$O + O + M$	$\rightarrow O_2 + M$	$1.2 \times 10^{-32} (300/T)^{2}$ [d,e]	*Nair et al.* [1994]
$O + O_2 + M$	$\rightarrow O_3 + M$	$1.5 \times 10^{-33} (300/T)^{2.4}$ [d,e]	*Sander et al.* [2003]
$O + O_3$	$\rightarrow O_2 + O_2$	$8.0 \times 10^{-12} e^{-2060/T}$	*Sander et al.* [2003]
$OH + OH$	$\rightarrow H_2O + O$	$4.2 \times 10^{-12} e^{-240/T}$	*Sander et al.* [2003]
$O(^1D) + N_2$	$\rightarrow O(^3P) + N_2$	$1.8 \times 10^{-11} e^{110/T}$	*Sander et al.* [2003]
$O(^1D) + O_2$	$\rightarrow O(^3P) + O_2$	$3.2 \times 10^{-11} e^{70/T}$	*Sander et al.* [2003]
$CO + OH$	$\rightarrow CO_2 + H$	$1.5 \times 10^{-13} (1+0.6p)$ [g]	*Sander et al.* [2003]
$CO + O + M$	$\rightarrow CO_2 + M$	$2.2 \times 10^{-33} e^{-1780/T}$	*Inn* [1974]
$H + CO + M$	$\rightarrow HCO + M$	$2.4 \times 10^{-31} e^{-1370/T}$ [d,e,h]	*Baulch et al.* [1994]
$H + HCO$	$\rightarrow H_2 + CO$	1.8×10^{-10}	*Friedrichs et al.* [2002]
$HCO + HCO$	$\rightarrow H_2CO + CO$	4.5×10^{-11}	*Friedrichs et al.* [2002]
$OH + HCO$	$\rightarrow H_2O + CO$	1.7×10^{-10}	*Baulch et al.* [1992]
$O + HCO$	$\rightarrow H + CO_2$	5.0×10^{-11}	*Baulch et al.* [1992]
$O + HCO$	$\rightarrow OH + CO$	5.0×10^{-11}	*Baulch et al.* [1992]
$H_2CO + H$	$\rightarrow H_2 + HCO$	$2.14 \times 10^{-12} e^{-1090/T}$	*Baulch et al.* [1994]
$H + H + M$	$\rightarrow H_2 + M$	$2.3 \times 10^{-32} (298/T)^{0.6}$ [d,e]	*Baulch et al.* [1992]
$HCO + O_2$	$\rightarrow HO_2 + CO$	5.2×10^{-12}	R. Atkinson et al.
$H_2CO + OH$	$\rightarrow H_2O + HCO$	9.0×10^{-12}	*Sander et al.* [2003]
$H + OH + M$	$\rightarrow H_2O + M$	$1.7 \times 10^{-30} (298/T)^{2}$ [c,e]	*Baulch et al.* [1992]
$OH + OH + M$	$\rightarrow H_2O_2 + M$	2.6×10^{-11} [c]	*Sander et al.* [2003]
		$1.7 \times 10^{-31} (300/T)$ [d,e]	*Sander et al.* [2003]
$H_2CO + O$	$\rightarrow HCO + OH$	$3.4 \times 10^{-11} e^{-1600/T}$	*Sander et al.* [2003]
$H_2O_2 + O$	$\rightarrow OH + HO_2$	$1.4 \times 10^{-12} e^{-2000/T}$	*Sander et al.* [2003]
$O(^1D) + CO$	$\rightarrow CO + O$	6×10^{-11} [i]	*Davidson et al.* [1978]
$CO_2 + O(^1D)$	$\rightarrow CO_2 + O$	$7.4 \times 10^{-11} e^{110/T}$	*Sander et al.* [2003]
$O_3 + O(^1D)$	$\rightarrow O_2 + O_2$	1.2×10^{-10}	*Sander et al.* [2003]
$O_3 + O(^1D)$	$\rightarrow O_2 + O + O$	1.2×10^{-10}	*Sander et al.* [2003]

Reactants	Products	Photolysis Rate[j]	Reference
$O_2 + h\nu$	$\rightarrow O(^3P) + O(^1D)$	1.1×10^{-6}	*Sander et al.* [2003]
$O_2 + h\nu$	$\rightarrow O(^3P) + O(^3P)$	2.1×10^{-8}	*Sander et al.* [2003]
$H_2O + h\nu$	$\rightarrow H + OH$	3.4×10^{-6}	*Sander et al.* [2003]
$O_3 + h\nu$	$\rightarrow O_2 + O(^1D)$	1.2×10^{-3}	*Sander et al.* [2003]
$O_3 + h\nu$	$\rightarrow O_2 + O(^3P)$	1.2×10^{-3}	*Sander et al.* [2003]
$H_2O_2 + h\nu$	$\rightarrow OH + OH$	2.8×10^{-5}	*Sander et al.* [2003]
$CO_2 + h\nu$	$\rightarrow CO + O(^3P)$	5.8×10^{-10}	*Sander et al.* [2003]
$H_2CO + h\nu$	$\rightarrow H_2 + CO$	1.8×10^{-5}	*Sander et al.* [2003]
$H_2CO + h\nu$	$\rightarrow HCO + H$	2.1×10^{-5}	*Sander et al.* [2003]
$HCO + h\nu$	$\rightarrow H + CO$	1×10^{-2}	assumed
$CO_2 + h\nu$	$\rightarrow CO + O(^1D)$	6.2×10^{-8}	*Sander et al.* [2003]
$HO_2 + h\nu$	$\rightarrow OH + O$	1.8×10^{-4}	*Sander et al.* [2003]

[a] Two-body rates are in $cm^3\ s^{-1}$; 3-body rates are in $cm^6\ s^{-1}$; photolysis rates $[s^{-1}]$.

[b] R. Atkinson et al. (Summary of evaluated kinetic and photochemical data for atmospheric chemistry, IUPAC Subcommittee on Gas Kinetic Data Evaluation for Atmospheric Chemistry, December 2001, available at http://rpw.chem.ox.ac.uk/IUPACsumm_web_latest.pdf).

[c] High density limit (k_∞) for three-body reaction $[cm^3\ s^{-1}]$.

[d] Low density limit for three-body reaction $[cm^6\ s^{-1}]$.

[e] The reported rate in air has been multiplied by a factor of 2.5 to account for CO_2 as third body [*Nair et al.*, 1994].

[f] The model is sensitive to this very uncertain branching ratio.

[g] The variable p is atmospheric pressure in bars.

[h] The model is sensitive to this very uncertain reaction rate.

[i] This is sometimes reported as an addition to form CO_2.

[j] Photolysis rates are evaluated at the top of the atmosphere $[s^{-1}]$ for a 57.3° slant path, and reduced by a factor of 2 to account for night.

Table 2. Nitrogen Reactions

Reactants	Products	Rate[a]	Reference[b]
H + NO + M	→ HNO + M	$2.4 \times 10^{-10}(300/T)^{0.4}$ [c]	*Tsang and Herron* [1991]
		$1.2 \times 10^{-31}e^{-210/T}$ (*c*)	*Tsang and Herron* [1991]
N + N + M	→ N_2 + M	$2.5 \times 1.25 \times 10^{-32}$ [d,e]	*Sander et al.* [2003]
N + O_2	→ NO + O	$1.5 \times 10^{-12}e^{-3600/T}$	*Sander et al.* [2003]
N + OH	→ NO + H	$3.8 \times 10^{-11}e^{85/T}$	R. Atkinson et al.
N + NO	→ N_2 + O	$2.1 \times 10^{-11}e^{100/T}$	*Sander et al.* [2003]
NO + O_3	→ NO_2 + O_2	$3.0 \times 10^{-12}e^{-1500/T}$	*Sander et al.* [2003]
NO + O + M	→ NO_2 + M	3.0×10^{-11} [c]	*Sander et al.* [2003]
		$2.3 \times 10^{-31}(300/T)^{1.5}$ [d,e]	*Sander et al.* [2003]
NO + HO_2	→ NO_2 + OH	$3.5 \times 10^{-12}e^{250/T}$	*Sander et al.* [2003]
NO + OH + M	→ HNO_2 + M	$3.6 \times 10^{-11}(300/T)^{0.1}$ [c]	*Sander et al.* [2003]
		$1.8 \times 10^{-30}(300/T)^{2.6}$ [d,e]	*Sander et al.* [2003]
NO_2 + O	→ NO + O_2	$5.6 \times 10^{-12}e^{180/T}$	*Sander et al.* [2003]
NO_2 + OH + M	→ HNO_3 + M	2.5×10^{-11} [c]	*Sander et al.* [2003]
		$5.0 \times 10^{-30}(300/T)^{3.0}$ [d,e]	*Sander et al.* [2003]
NO_2 + H	→ NO + OH	$4.0 \times 10^{-10}e^{-340/T}$	*Sander et al.* [2003]
HNO_3 + OH	→ H_2O + NO_2 + O	$2.4 \times 10^{-14}e^{460/T}$ [f]	*Sander et al.* [2003]
HNO_3 + OH + M	→ H_2O + NO_2 + O + M	$2.7 \times 10^{-17}e^{2200/T}$ [c,f]	*Sander et al.* [2003]
		$1.6 \times 10^{-33}e^{1335/T}$ [d,e,f]	*Sander et al.* [2003]
HCO + NO	→ HNO + CO	1.3×10^{-11}	*Nesbitt et al.* [1989]
H + HNO	→ H_2 + NO	$3.0 \times 10^{-11}e^{-500/T}$	*Tsang and Herron* [1991]
O + HNO	→ OH + NO	3.8×10^{-11}	*Inomata and Washida* [1999]
OH + HNO	→ H_2O + NO	5.0×10^{-11}	*Sun et al.* [2001]
HNO_2 + OH	→ H_2O + NO_2	$1.8 \times 10^{-11}e^{-390/T}$	*Sander et al.* [2003]
HO_2 + NO_2 + M	→ HO_2NO_2 + M	4.7×10^{-12} $(300/T)^{1.4}$ [c]	*Sander et al.* [2003]
		4.5×10^{-31} $(300/T)^{3.2}$ [d,e]	*Sander et al.* [2003]
OH + HNO_4	→ H_2O + O_2 + NO_2	$1.8 \times 10^{-11}e^{38/T}$	*Sander et al.* [2003][g]
O + HNO_4	→ HO_2 + HNO_3	$7.8 \times 10^{-11}e^{-3400/T}$	*Sander et al.* [2003][g]
HNO_2 + hν	→ NO + OH	1.7×10^{-3}	assumed
HNO_3 + hν	→ NO_2 + OH	4.3×10^{-5}	*Sander et al.* [2003]
NO + hν	→ N + O	1.8×10^{-6}	*Sander et al.* [2003]
NO_2 + hν	→ NO + O	2.24×10^{-3}	*Sander et al.* [2003]
HNO + hν	→ NO + H	1.7×10^{-3}	assumed

[a]Two-body rates [cm^3 s^{-1}]; three-body rates [cm^6 s^{-1}]; photolysis rates [s^{-1}].
[b]R. Atkinson et al. (Summary of evaluated kinetic and photochemical data for atmospheric chemistry, IUPAC Subcommittee on Gas Kinetic Data Evaluation for Atmospheric Chemistry, December 2001, available at http://rpw.chem.ox.ac.uk/IUPACsumm_web_latest.pdf).
[c]High density limit (k_∞) for 3-body reaction [cm^3s^{-1}].
[d]Low density limit for 3-body reaction [cm^6s^{-1}].
[e]The reported rate in air has been multiplied by a factor of 2.5 to account for CO_2 as third body [*Nair et al.*, 1994].
[f]The reaction of OH and HNO_3 has multiple channels; see *Sander et al.* [2003] for details.
[g]Products assumed.

escape from Mars seems to be quite close to the diffusion limit. Aeronomical details do not matter if escape is diffusion-limited.

3.1.1. Diffusion-Limited Flux

[16] The diffusion-limited flux $\phi_{\rm lim}$ is the highest possible in a hydrostatic atmosphere [*Hunten*, 1974]. The diffusion limit can be written

$$\phi_{\rm lim} = f_{\rm tot}({\rm H}) b_{aj}\left(\frac{1}{H_a} - \frac{1}{H_j}\right), \qquad (1)$$

where $f_{\rm tot}$(H) is the total hydrogen mixing ratio in the stratosphere (adequately approximated by $2f(H_2)$ for Mars), b_{aj} is the binary diffusion coefficient between CO_2 and the escaping species j, and H_a and H_j are the scale heights of CO_2 and j. The binary diffusion coefficient between H_2 and CO_2 is approximated by [*Marrero and Mason*, 1972]

$$b_{aj}({\rm CO_2, H_2}) = \frac{31.4}{k_{\rm B}} T^{0.75} e^{-11.7/T} \left[{\rm cm^{-1}\ s^{-1}}\right], \qquad (2)$$

where $k_{\rm B}$ is the Boltzmann constant and the temperature T is in K. To our knowledge the binary diffusion coefficient between H and CO_2 has not been measured; we take it to be 1.8× bigger than for H_2 in CO_2, which is the ratio of binary diffusion coefficients of H and H_2 in helium [*Marrero and Mason*, 1972].

[17] *Krasnopolsky and Feldman* [2001] report that the H_2 abundance in the lower atmosphere is 17 ppm. The corresponding diffusion-limited flux would be 3.7×10^8 H atoms cm^{-2} s^{-1}. This is only about 50% bigger than the conventional estimate of 2.4×10^8 H atoms cm^{-2} s^{-1} [*Nair et al.*, 1994]. The near coincidence is a broad hint that H escape is diffusion-limited.

[18] Diffusion-limited escape is naturally expressed as a velocity. The diffusion-limited velocity is $v_{\rm lim} = \phi_j/(f_j N_a)$. This is applied at the top of the grid:

$$v_{\rm lim} = \frac{b_{aj}}{N_a}\left(\frac{1}{H_a} - \frac{1}{H_j}\right). \qquad (3)$$

In equation (3), the density N_a refers to the atmospheric density [cm^{-3}] at the altitude where $v_{\rm lim}$ is being evaluated. In our model we evaluate $v_{\rm lim}$ and N_a at 110 km.

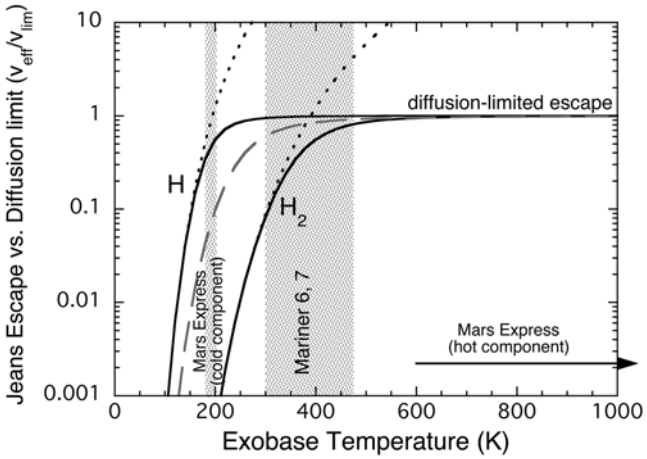

Figure 2. Diffusion-limited Jeans escape (solid lines) for H and H_2 as functions of exobase temperature. These are the end members. Uncorrected Jeans escape (dotted curves) is shown for comparison. The intermediate case shows diffusion-limited Jeans escape in which 10% of the H_2 is converted to H at the exobase. The shaded region represents the range of Mariner 6 and 7 temperatures; the Mars Express high-temperature component is reported as ~1000 K but with no useful upper bound [*Galli et al.*, 2006b].

[19] We can define a general hydrogen effusion velocity $v_{\rm eff}$ at the top of the grid by analogy to $v_{\rm lim}$. In the absence of chemical sources and sinks, the ratio $v_{\rm eff}/v_{\rm lim}$ is constant. We define effusion velocities for H and H_2 at 110 km.

3.1.2. Jeans Escape

[20] It is interesting to consider how diffusion interacts with Jeans escape. Jeans escape is evaluated at the exobase, the altitude above which atmospheric atoms and molecules no longer collide with each other [*Jeans*, 1925; *Walker*, 1977].

$$\phi_{\rm je} = f_e N_e \sqrt{\frac{kT}{2\pi m_j}} \left(1 + \frac{R_e}{H_j}\right) e^{-R_e/H_j}, \tag{4}$$

where N_e and f_e refer to the exobase density and the hydrogen mixing ratio at the exobase, respectively, and R_e refers to the location of the exobase. In the limit where escape is small and hydrogen a minor constituent, the exobase is defined by the major constituent. It is usual to define N_e by setting the mean free path equal to the scale height H_a.

[21] The hydrogen mixing ratio at the exobase f_e is related to the total hydrogen mixing ratio at the homopause $f_{\rm tot}$(H) by integrating the diffusion equation [*Zahnle et al.*, 1990]; a simple analytic solution is obtained if we assume an isothermal atmosphere and ignore eddy diffusion above the homopause.

$$\frac{f_e}{f_{\rm tot}({\rm H})} = \frac{\phi_{\rm je}}{\phi_{\rm lim}} + \left(1 - \frac{\phi_{\rm je}}{\phi_{\rm lim}}\right) \exp\left\{(R_e - R_h)\left(\frac{1}{H_a} - \frac{1}{H_j}\right)\right\}. \tag{5}$$

One usually thinks of a species as relaxing to its own scale height above the homopause, but this is not so for hydrogen in diffusion-limited escape. Rather, escape reduces the scale height, and in the diffusion limit $f_e \rightarrow f_{\rm tot}$. Equations (1), (4), and (5) can be solved for the ratio $\phi_{\rm je}/\phi_{\rm lim}$. The altitude of the exobase is $R_e = R_h + H_a \ln (N_a/N_e)$ in the isothermal atmosphere. For $m_j \ll m_a$, the binary diffusion coefficient is related to the mean free path H_a and the thermal velocity $\bar{c} = \sqrt{8kT/\pi m_j}$ by $b_{aj} \approx \frac{1}{3} H_a \bar{c} N_e$ [*Jeans*, 1925, pp. 312–314]. The result is

$$\frac{\phi_{\rm lim}}{\phi_{\rm je}} = 1 - \left(\frac{4}{3}\frac{(1 - H_a/H_j)e^{R_e/H_j}}{(1 + R_e/H_j)} - 1\right) \cdot \exp\left\{(R_e - R_h)\left(\frac{1}{H_a} - \frac{1}{H_j}\right)\right\}. \tag{6}$$

Two end-member cases are plotted on Figure 2, one in which all H_2 is photochemically dissociated into atomic H (labeled H), and the other where H_2 escapes as H_2. The true situation lies somewhere between, in which hydrogen escapes mostly or entirely as H but most of the hydrogen is in the form of H_2. An arbitrary intermediate example, in which 10% of the H_2 is converted to H at the exobase, is shown for illustration. Figure 2 makes the general point that for plausible conditions on Mars, the hydrogen escape rate should approach the diffusion limit.

3.1.3. Current Hydrogen Escape

[22] Hydrogen escape fluxes are not observed directly, a point emphasized by *Hunten* [1990]. Rather, they are (for Mars) inferred from the altitude profile of atomic hydrogen above the exobase, which has itself been obtained by inverting limb soundings of scattered solar Lyα. For Mars the best data were obtained by Mariners 6 and 7. *Anderson and Hord* [1971] described their inferred atomic hydrogen profile in terms of a density and temperature at the exobase. They assumed that the hydrogen atoms obeyed a Maxwellian velocity distribution at the exobase to obtain the spatial distribution of hydrogen atoms, taking into account that some hydrogen atoms would be in satellite or escape orbits. Anderson and Hord's exobase parameters are given in Table 3. The corresponding Jeans escape flux is 1.5–1.8 × 10^8 atoms cm^{-2} s^{-1}, but given the uncertainty in the temperature, 350 ± 100 K, the Jeans flux is uncertain to a factor of 2. *Nair et al.* [1994] deduced a total hydrogen

Table 3. Inferred H Escape Fluxes

Model	Spacecraft	$n_{\rm exo}$(H) [cm^{-3}]	$T_{\rm exo}$ [K]	$\phi_{\rm je}$ [cm^{-2} s^{-1}]
Anderson and Hord [1971]	Mariner 6	$3 \pm 1 \times 10^4$	350 ± 100	$1.8^{+2.2}_{-1.4} \times 10^8$
Anderson and Hord [1971]	Mariner 7	$2.5 \pm 1 \times 10^4$	350 ± 100	$1.5^{+1.7}_{-1.2} \times 10^8$
Galli et al. [2006b]	Mariner 6	$7.1^{+0.7}_{-1.6}$ 1×10^4	350^{+100}_{-50}	$4.1^{+5.4}_{-2.0} \times 10^8$
Galli et al. [2006b]	Mariner 7	$3.4^{+1.6}_{-0.5} \times 10^4$	425 ± 100	$3.8^{+2.5}_{-1.3} \times 10^8$
Galli et al. [2006b]	Mars Express	$6.4^{+4.6}_{-0.6} \times 10^3$	1000^{+1000}_{-400}	$4.3^{+5.6}_{-2.5} \times 10^8$

escape flux of 2.4×10^8 by tuning their photochemical model to give Anderson and Hord's H densities and then adding to this Jeans escape by H_2 at the same temperature as H.

[23] Aerobraking experienced by more recent spacecraft suggests that the Martian exosphere as a whole is considerably colder, closer to ~200 K than to ~350 K [*Lichtenegger et al.*, 2006]. The colder background atmosphere suggests that the atomic hydrogen is better described by two populations, one at the atmospheric temperature of ~200 K, and the other warm or hot. A similar effect has been inferred on Venus, where there also appear to be two different populations of exospheric hydrogen, one of which is hot and dominates escape [*Donahue et al.*, 1997]. In neither case is the origin of the hot H fully understood. Possibilities include charge exchange with solar wind protons and dissociative reactions between H_2 and CO_2^+ and O^+ that make hot H atoms [*Galli et al.*, 2006a, 2006b; *Lichtenegger et al.*, 2006]. It is also probable that the "double-humped" non-Maxwellian velocity distribution function for H atoms above the exobase [*Barakat et al.*, 1995] is better approximated by two Maxwellians than by one Maxwellian.

[24] *Galli et al.* [2006b] fit two-component models both to new data from Mars Express and to the old Mariner 6 and 7 data. Galli et al. base their H profiles on 1D Monte Carlo modeling of atoms at and above the exobase. The Monte Carlo models do not presume that the velocity distribution function is Maxwellian. Their results are reported in Table 3. Applied to the Mariner data, Galli et al.'s model gives somewhat denser or warmer conditions than *Anderson and Hord*'s [1971]. Mars Express encountered distinctly different conditions than did the two Mariners. Galli et al.'s best fit to the Mars Express data is both hotter (~1000 K) and thinner. A key point is that all three of Galli et al.'s fits give the same Jeans escape flux of $\sim 4 \times 10^8$ atoms cm^{-2} s^{-1}, despite markedly different temperatures. Such a coincidence is expected of diffusion-limited escape, where escape is limited deep in the atmosphere, but not of temperature-limited escape, for which escape would be higher when the temperature is higher. Moreover, and quite independently, the deduced escape flux is close to the expected diffusion-limited escape flux of 3.5×10^8 atoms cm^{-2} s^{-1} for 17 ppm H_2.

[25] Other workers have also found that a Maxwellian velocity distribution can underestimate densities above the exobase, and hence underestimate escape. *Barakat and Schunk* [2007] compared Monte Carlo simulations of the distribution of a trace low mass constituent above an exobase to results obtained using various fluid dynamic approximations, including the usual 5-moment approximation and Grad's 13-moment approximation. The Monte Carlo simulations are presumably most nearly correct. Barakat and Schunk found that the familiar 5-moment approximation, which is derived from the Boltzmann equation by assuming a Maxwellian velocity distribution to close the system of moment equations [*Schunk*, 1975], underestimates the number density of the low mass trace species by about a factor of 2. Grad's 13-moment approximation, which uses a complicated, non-Maxwellian velocity distribution to close the system of moment equations [*Schunk*, 1975], does quite well. *Cui et al.* [2008] applied Grad's 13-moment approximation to diffusion-limited escape of H_2 from Titan. Temperatures and densities in Titan's exosphere are obtained directly by in situ sampling with the Cassini spacecraft. *Cui et al.* [2008] deduce a hydrogen escape flux 2.5× higher than what simple Jeans escape predicts.

[26] The higher densities seen in *Galli et al.*'s [2006b] models are consistent with these other results. The more accurate velocity distribution functions, such as Grad's, have more fast moving, outbound atoms than does the Maxwellian. The net result is that *Anderson and Hord*'s [1971] Maxwellian H profile is likely to underestimate the hydrogen abundance above the exobase, and hence underestimate how fast hydrogen escapes from Mars, compared to Galli et al.'s more nuanced model.

[27] We conclude that at present, the totality of the evidence suggests that hydrogen escape from Mars is diffusion-limited, and therefore rather higher than it has usually been taken to be. We suspect that relatively low H escape rates have been favored historically because they have been tethered to the theoretical construct that H escape must be balanced by O escape, and many studies have consistently shown that the O escape rate is small [*Lammer et al.*, 2003]. We therefore repeat our agreement with *Lammer et al.* [2003]: the main sink on O is at the surface. The H escape rate is then freed to reach the diffusion limit. Diffusion-limited escape is an important simplification that reduces our models to a one-parameter family.

3.2. Oxygen Deposition

[28] As a first approximation, we implement dry deposition by assuming a single deposition velocity v_{dep} that we apply to all reactive gases. In the current Martian atmosphere, hydrogen peroxide (H_2O_2) and ozone (O_3) are the most important reactive gases. Both are strong oxidants that by entering the soil make the soil strongly oxidizing as well. We show below that our models work best with $0.01 < v_{dep} < 0.03$ cm s^{-1}. This is much smaller than the corresponding deposition velocities on Earth. For comparison, v_{dep} for H_2O_2 and O_3 over continents are about 1.0 and 0.07 cm s^{-1}, respectively [*Seinfeld and Pandis*, 2006]. It is expected that v_{dep} would be higher for these gases on Earth where liquid water is a common surface.

[29] *Bullock et al.* [1994] addressed the diffusion and reaction rates of H_2O_2 in Martian soils. They considered two end-member cases, one with the least H_2O_2 in the soil that can account for the Viking observations, the other imposing the characteristic 10^5–10^7 year loss timescale deduced by *Chyba et al.* [1989] from the thermal sensitivity seen in the Viking labeled release experiments. If we use the same parameters that Bullock et al. used in their model, we find that their results can be described by H_2O_2 deposition velocities between 0.03 cm s^{-1} (10^5 year timescale) to 0.6 cm s^{-1} (minimum H_2O_2). Our photochemical models predict about 6× more H_2O_2 in the atmosphere near the surface than Bullock et al. assumed, which suggests that v_{dep} should be 6× smaller. The corresponding range of dry deposition velocities is $0.005 < v_{dep} < 0.1$ cm s^{-1}. Our results are consistent with this range.

[30] A consequence of applying a deposition velocity to H_2O_2 is that the surface must be a net sink of H_2O_2. In other words, our construction implicitly assumes that peroxides eventually react with ferrous iron or reduced sulfur to make ferric iron and sulfate. Accumulated over 4 Ga, the average thickness of the oxidized rind would be tens of meters

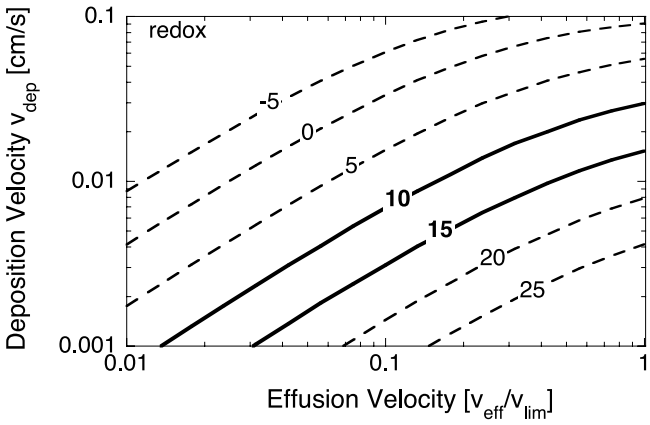

Figure 3. Contours (in μbar) of constant net oxidation in steady state as a function of the upper and lower boundary conditions for a 6.3 mbar CO_2 atmosphere with 9.5 μm of water vapor. Net oxidation is defined as $p\mathrm{Ox} \equiv 2p\mathrm{O}_2 - p\mathrm{CO} - p\mathrm{H}_2$. The boundary conditions are the hydrogen effusion velocity v_{eff} (as a fraction of v_{lim}) and the deposition velocity v_{dep} of highly reactive species. Current Mars has $p\mathrm{Ox} \approx 10$–15 μbar. Our preferred models presume diffusion-limited H escape, for which $v_{\mathrm{eff}}/v_{\mathrm{lim}} = 1$.

(much less if starting from pyrite or elemental sulfur, a bit more if starting from olivine). This seems reasonable, if not proved. Spacecraft observations show that olivine minerals are present on the surface of Mars, which indicates that ferrous iron remains readily available to be oxidized today. Olivine has been observed in situ by the Thermal Emission Spectrometer (mini-TES) and Mossbauer spectrometers on the Mars Exploration Rovers and is present in the soil in the form of basaltic sand at both landing sites of Meridiani Planum and Gusev Crater [*McSween et al.*, 2006; *Klingelhofer et al.*, 2006; *Morris et al.*, 2006]. Mars Express observations also indicate that olivine-rich restricted areas occur in rims and floors of craters [*Mustard et al.*, 2005], while Thermal Emission Imaging System (THEMIS) observations indicate that the largest deposit of olivine is in Nili Fossae [*Hoefen et al.*, 2003]. Gas-solid oxidation reactions are likely to occur over time, through adsorption mechanisms, downward diffusion, and the exposure of fresh material from impacts [*Huguenin*, 1973; *Zent*, 1998].

[31] Oxidation is a long-term sink, representing the global average on a 10^5 year timescale. H_2O_2 in the atmosphere has a short photochemical lifetime of less than a day. It is expected to be, and inferred from observations to be, highly variable in space and time. Although surface deposition of H_2O_2 is important to the redox state of the atmosphere as a whole on long timescales, it is a relatively small term compared to the gas phase chemical reactions that daily create and destroy H_2O_2, and hence v_{dep} has no significant effect on H_2O_2 atmospheric abundance.

3.3. Oxygen Escape

[32] At present O escape does not appear to be important for Mars [*Lammer et al.*, 2003]. However, the consensus is that O escape was vastly greater in the past, as a consequence of higher solar EUV radiation and much bigger solar winds [*Luhmann*, 1997; *Lammer et al.*, 2003]. An oxygen escape flux of 10^7 cm^{-2} s^{-1} today might scale to escape fluxes as high as 10^8 cm^{-2} s^{-1} 2.5 Ga and 10^9 cm^{-2} s^{-1} at 3.5 Ga [*Lammer et al.*, 2003]. At 10^9 cm^{-2} s^{-1}, oxygen escape provides a reducing force on the atmosphere that would be of the same order of magnitude as volcanic activity at levels seen on Earth today. At these rates of escape, O escape becomes a major driver on the atmosphere.

[33] Oxygen escape to space is not expected to depend strongly on the oxidation state of the atmosphere, at least not while CO_2 is the major constituent of the atmosphere, because the ultimate source of the escaping O is CO_2. This means that O escape is not subject to the obvious strong negative feedbacks that oxygen deposition to the surface is subject to. Predicted high rates of O escape would seem to guarantee that the atmosphere become reducing. We will address these matters in more detail in sections 5.3, 5.4, and 6.

4. Results for Current Mars

[34] Models are run to steady state. We typically run a model for 10^{15} years, which is a ridiculously long time, but well suited to obtaining a true steady state. A balanced redox budget provides a test of the model's self-consistency. Our models balance the fluxes in the redox budget to about 1 ppm, with some variation from run to run. Put another way, unaccounted imbalances in the redox budget are on the order of 10^{-6} of the H escape flux. Because the H_2 mixing ratio depends mostly on H escape, this is equivalent to converging the H_2 mixing ratio to 0.0001%.

[35] Basic model results are illustrated by Figures 3–6 and summarized in Table 4. Figure 3 shows contours of net oxidation $p\mathrm{Ox} \equiv 2p\mathrm{O}_2 - p\mathrm{CO} - p\mathrm{H}_2$ as functions of the v_{dep} and v_{eff}. Currently, $10 < p\mathrm{Ox} < 15$ μbar. Our preferred models use $v_{\mathrm{eff}} = v_{\mathrm{lim}}$, the diffusion limit, which is the maximum possible value for v_{eff}.

[36] Figure 4 shows how various properties of the atmosphere change along a fixed pOx contour. It is notable that the CO and O_2 mixing ratios change very little while the strength of the forcing from the boundary conditions varies over 2 orders of magnitude. The main effects of the

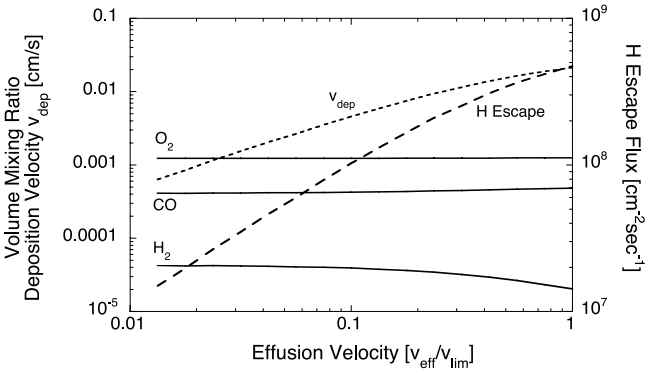

Figure 4. How certain key observables vary along the $p_{\mathrm{Ox}} = 12.5$ μbar contour as a function of v_{eff} for a 6.3 mbar CO_2 atmosphere with 9.5 μm of water vapor. Deposition velocity and mixing ratios are plotted against the left-hand axis. The hydrogen escape flux is plotted against the right-hand axis.

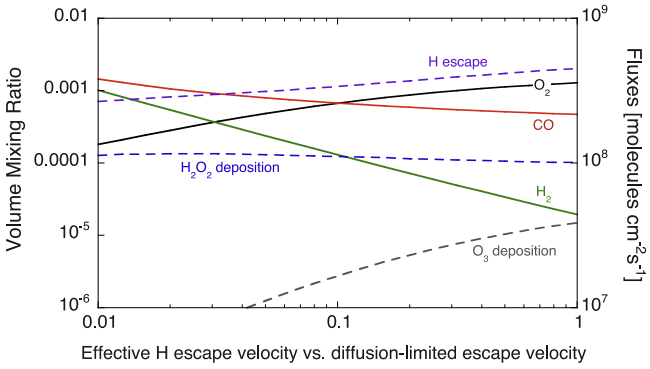

Figure 5. How certain key observables vary with the hydrogen effusion velocity (v_{eff}/v_{lim}) when the dry deposition velocity is held fixed. Here $v_{dep} = 0.02$ cm s^{-1} for all reactive species. By assumption $v_{dep} = 0$ for CO, O_2, and H_2.

boundary conditions are on hydrogen escape and the H_2 mixing ratio. The reported H_2 mixing ratio of 17 ppmv [*Krasnopolsky and Feldman*, 2001] is approached in the limit that $v_{eff} \rightarrow v_{lim}$. This demands a hydrogen escape rate of $\sim 4 \times 10^8$ H atoms cm^{-2} s^{-1}. Lower hydrogen escape fluxes correspond to greater amounts of H_2 in the atmosphere. The corresponding deposition velocity $v_{dep} = 0.02$ cm s^{-1}. This is model A in Table 4.

[37] Figure 5 addresses how easily H escapes by changing v_{eff} while v_{dep} is held fixed at 0.02 cm s^{-1}; this is effectively the partial derivative of the model with respect to v_{eff}. Lowering v_{eff} makes the atmosphere more reducing. The loss of oxidant to the surface is chiefly through H_2O_2. This changes little as a function of v_{eff} while v_{dep} is fixed. Evidently, the H_2O_2 ground level mixing ratio is insensitive to how easily H escapes. Consequently the H escape flux changes little, and so the biggest response of the atmosphere to changing v_{eff} is to make a compensating change in the H_2 mixing ratio. Atmospheres with low v_{eff} have more H_2 and are more reducing.

[38] Figure 6 addresses the strength of the surface sink by changing v_{dep}, while leaving v_{eff} fixed at the diffusion limit. This is effectively the partial derivative of the model with respect to v_{dep}. Raising v_{dep} makes the atmosphere more reducing. Again, the loss of oxidant to the surface is chiefly through H_2O_2, and because the H_2O_2 ground level mixing ratio is insensitive to how easily H escapes, the oxygen sink is proportional to v_{dep}. Bigger losses of H_2O_2 to the surface require bigger losses of H to space, which for fixed v_{eff} is accomplished by raising $f(H_2)$. The shading indicates the range of models generally consistent with modern Mars. Model A in Table 4 is for $v_{dep} = 0.02$ cm s^{-1}, in the middle of the shaded region.

[39] Table 4 compares our nominal model results to other published models and to Mars. Our nominal photochemical model (model A) does a good job with O_2, H_2, and H_2O_2, while falling a little short with CO. The simplest way to improve the agreement with CO is to consider a drier stratosphere. Model B shows that a globally averaged relative humidity of 17% (the average relative humidity at the ground), if imposed at all altitudes, raises the CO abundance to match what is observed without affecting the other major photochemical products. The success of model B suggests that the Martian stratosphere might be rather dry. To create a dry stratosphere would seem to require efficient atmospheric circulation through effective cold traps; this is not a good problem for a 1D model. It would be better addressed with a GCM.

[40] There are enough differences between our models and other published models that direct comparisons are difficult to make. These differences include temperature structure, eddy diffusion, chemical reaction rates, boundary conditions, and numerical convergence. In our models the H_2 mixing ratio is a chemical product that we predict. Our model predicts that the H_2 mixing ratio should be $\sim$20 ppmv

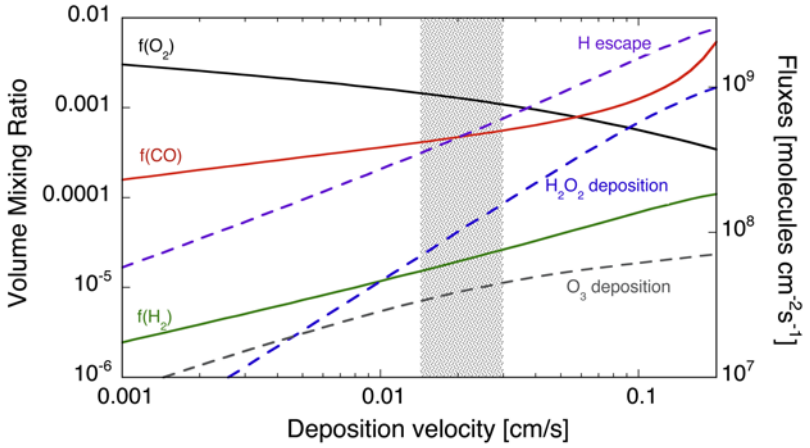

Figure 6. How certain key observables vary with deposition velocity (v_{dep}) when the escape velocity is held fixed at the limiting flux ($v_{eff} = v_{lim}$). All reactive atmospheric species are subject to the same value of v_{dep}, while $v_{dep} = 0$ for CO, O_2, and H_2. The shading indicates the range of v_{dep} that provides a good match to the Martian atmosphere. The model breaks down for $v_{dep} > 0.2$ cm s^{-1}: the surface oxygen sink becomes so big that reducing sinks become saturated and the CO mixing ratio increases dramatically; pCO_2 is set to 6.28 mbar. The CO runaway may be artificial because we have not included a surface sink on CO.

Table 4. Comparison of Mars Atmospheric Composition to Photochemical Models[a]

Variable	Units	Mars	Model A	Model B	Model C	Nair94	VK95	VK06
v_{dep}	cm s^{-1}		0.02	0.02	0.02			
v_{eff}/v_{lim}			1.0	1.0	1.0			
T_{surf}	K		211	211	201	215	215	215
CO_2	mbar	6.3	6.3	6.3	6.3	6.36	6.36	6.1
H_2O	ppt μm	10	9.5	9.5	9.5	8.8	9.5	10
O_2	ppmv	1200–2000	1300	1300	1650	1200	1150	1740
CO	ppmv	800	470	750	21400	470	540	112
H_2	ppmv	17	20	19	110	37	51	17[b]
H_2O_2	ppbv	20 ± 20[c]	24	24	40	21	20	12
pOx	μbar	10–20	13.3	11.5	−110	11.9	10.7	21.0
H esc.	$cm^{-2}s^{-1}$	$2–5 \times 10^8$	4.5×10^8	4.4×10^8	2.5×10^9	2.4×10^8	2.4×10^8	2.5×10^8
O esc.	$cm^{-2}s^{-1}$	$< 1 \times 10^7$	1×10^7	1×10^7	1×10^9	1.2×10^8	1.2×10^8	1.25×10^8
H_2O_2 dep	$cm^{-2}s^{-1}$	—	1.0×10^8	9.8×10^7	1.7×10^8	0	0	0
O_3 dep	$cm^{-2}s^{-1}$	—	3.9×10^7	3.9×10^7	2.8×10^7	0	0	0

[a]Mars data are from *Krasnopolsky* [2006]. Model A is our nominal model. Model B differs from model A by setting the relative humidity in the atmosphere equal to what it is at the ground. Model C applies model A to solar conditions 3.5 Ga (sections 5.3 and 5.4). *Nair et al.* [1994] (Nair94) changes two key chemical reaction rates at low temperatures to improve the model's agreement with observation. *Krasnopolsky* [1995] (VK95) includes a heterogenous sink on odd H species to better preserve CO; *Krasnopolsky* [2006] (VK06) refers to his model 1, gas-phase chemistry only. VK06 imposes both H escape and H_2 mixing ratio as boundary conditions, which implies that v_{eff} is an adjustable parameter in this model.

[b]VK06 fixes the H_2 mixing ratio as a boundary condition.

[c]H_2O_2 abundances are variable owing to a photochemical lifetime of less than a day.

if and only if escape is diffusion-limited. This is shown in Figures 4 and 5.

5. Historic and Ancient Mars

[41] The Martian atmosphere is not compositionally constant. The amounts of H_2O and CO_2 in the atmosphere change seasonally. It is likely that H_2O and CO_2 evolve in response to obliquity variations and other changing orbital parameters, volcanism, the evolving Sun, and sundry other factors. Here we consider how the steady state photochemistry responds to changing levels of H_2O, CO_2, and the linked affects of the evolving solar UV radiation and solar wind. As a first step we will in effect take the partial derivatives of our standard model with respect to H_2O, CO_2, and UV. For this exercise we treat CO_2, H_2O, and the Sun as independent variables. We hold the other boundary conditions constant; in particular H escapes in the diffusion limit and H_2O_2 and O_3 are delivered to the surface with $v_{dep} = 0.02$ cm s^{-1}.

5.1. Changing CO_2

[42] Figure 7 shows how our nominal model responds to changes in pCO_2. Temperature structure, relative humidity, eddy diffusivity, and boundary conditions are the same as for model A. The general trend is that the atmosphere becomes more oxidized as it gets thinner, and more reduced as it gets thicker. The chief reason for this is that water vapor photolysis is relatively more important in the thinner atmosphere. This is because there is less CO_2 but the same amount of water vapor (which depends on surface temperature). Therefore there is more OH in the thinner atmosphere. With more OH there is less CO (CO + OH → H + CO_2 is the chief reaction destroying CO) and more O_2 (O + OH → H + O_2 is the chief reaction making O_2). Conversely, a thicker CO_2 atmosphere reduces the relative importance of H_2O photolysis, which favors CO over O_2.

[43] Thinner CO_2 atmospheres than today are not discussed as often as thicker atmospheres. At times of low obliquity it is expected that the polar caps expand and pCO_2 drop to as low as a millibar [*Toon et al.*, 1980; *Manning et al.*, 2006]. We find that in steady state, such an atmosphere would be 2% O_2. It is unlikely that such episodes would leave an observable chemical imprint, given that the current atmosphere is quite oxidizing as is.

[44] Thick CO_2 atmospheres have been widely posited to explain fluvial features of ancient Mars [*Pollack et al.*, 1987; *Haberle*, 1998; *Forget and Pierrehumbert*, 1997]. Even today, at times of higher obliquity, it is possible that pCO_2 will increase significantly if there exist hidden stores of CO_2 that can be easily mobilized [*Nakamura and Tajika*, 2003; *Manning et al.*, 2006]. We find that for $pCO_2 \approx$ 10 mbar, CO is as abundant as O_2. Atmospheres with $pCO_2 > 50$ mbar begin to look rather poisonous. As pCO_2 approaches 100 mbar the atmosphere becomes unstable with respect to CO. Many discussions of early Mars have

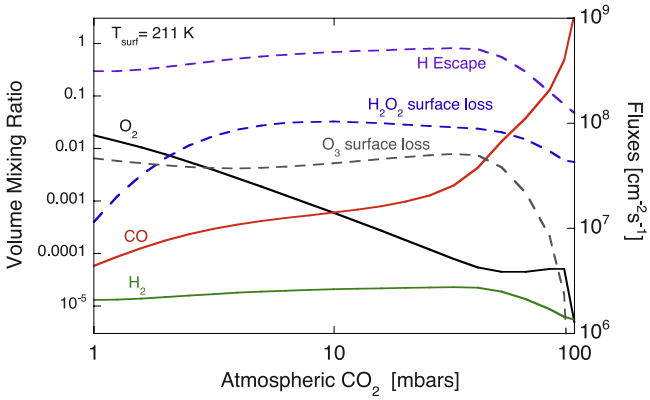

Figure 7. The effect of changing pCO_2 in the nominal model. These are steady state solutions. Both CO and O_2 are sensitive to pCO_2. Low pCO_2 generates more oxidized atmospheres, while higher pCO_2 generates more reduced atmospheres. The nominal model predicts that CO_2 becomes less stable than CO for $pCO_2 > 100$ mbar. The chemical state of the Martian atmosphere is likely to vary greatly on obliquity timescales.

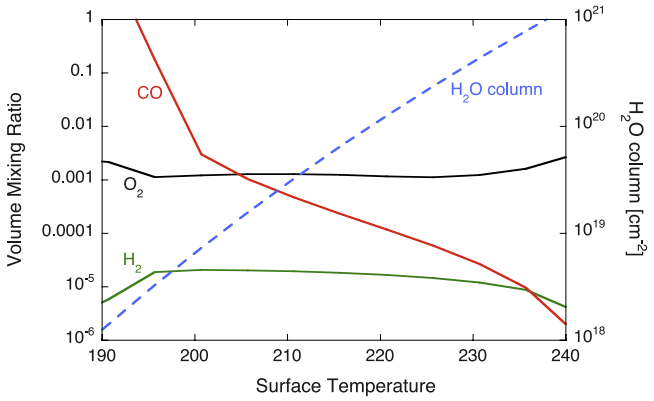

Figure 8. The atmospheric H_2O column supported by a given surface temperature on the right and the corresponding steady state O_2, CO, and H_2 volume mixing ratios on the left. CO abundance is sensitive to water vapor, but O_2 and H_2 are not. The nominal surface temperature circa 4 Ga would be 195 K.

confidently assumed that at least this much CO_2 was once present (see review by *Haberle* [1998]). Yet the photochemistry suggests that such an atmosphere might not be stable.

[45] What is going wrong for CO_2 in Figure 7 is that (1) the atmosphere is very dry and (2) the oxygen sink depends on H_2O_2 and O_3, which are made by three-body reactions and therefore easier to make in a denser atmosphere. Thus increasing CO_2 tends to make the atmosphere more reducing. The safety valve should be H escape, but H escape is insensitive to CO; meanwhile, the lack of water vapor lets CO build up.

[46] A weakness of these models is that they have only atmospheric gas phase sinks for CO. The models neglect surface sinks that might remove CO. Given that gas-phase photochemistry models tend to predict too little CO, additional major surface sinks are unlikely to be very important today. But surface sinks would almost certainly become important if CO were a major gas. CO has a well-known affinity for Fe, and Fe is abundant in surface minerals on Mars. At some level, minerals might catalyze the reaction of CO with photochemically generated H_2O_2 and O_3 to make CO_2.

5.2. Changing H_2O

[47] Atmospheric composition is sensitive to absolute humidity. Like pCO_2, humidity is expected to vary as the obliquity, eccentricity, and longitude of perihelion precess. For simplicity we vary atmospheric water vapor by raising and lowering the temperature, holding relative humidity constant. The atmosphere is held to pCO_2 = 6.28 mbar, and other boundary conditions are the same as in model A. This is a relatively crude approach but it is adequate to illustrate the sensitivities.

[48] Figure 8 gives both the surface temperature and the corresponding water column as the independent variable. To first approximation, the CO/CO_2 ratio is inversely proportional to the amount of water vapor in the atmosphere, as expected. The apparent sensitivity of CO to surface temperature is almost entirely attributable to the water vapor abundance. Photochemical products of water vapor act as catalysts that help O_2 and CO recombine to CO_2. The model predicts that CO replaces CO_2 as the major C-bearing gas for $T < 192$ K. This prediction is interesting but should not be taken very seriously because it depends on the presumption that the boundary conditions that describe the current atmosphere remain applicable to the colder atmosphere. In particular, surface sinks on CO are neglected, which may be unrealistic when CO has become a major gas.

5.3. The Young Sun

[49] The young Sun was a stronger source of photolytically active UV radiation and a much stronger source of solar wind than it is today [*Lammer et al.*, 2003]. Oxygen escape cannot be neglected under these conditions. For simplicity we have combined these effects in a single parameter. We scale UV photolysis rates at short wavelengths ($\lambda < 175$ nm) as the square root of the O escape rate, and at longer wavelengths as the 0.3 power of O escape. These are arbitrary scalings that reflect the relative sensitivities of the different phenomena to the young Sun. *Lammer et al.* [2003] suggest that the O escape flux was $\sim 10^9$ cm^{-2} s^{-1} at circa 3.5 Ga. We vary O escape from 10^7 cm^{-2} s^{-1} today to 10^{10} cm^{-2} s^{-1}. Other model parameters are held fixed.

[50] Figure 9 shows the result of doing these things. The response of the atmosphere is dominated by O escape, which is the forcing that changes the most. Oxygen escape generates a more reduced atmosphere, which favors CO. Increased UV photolysis acting alone simply raises the abundances of the photochemical products (O_2, CO, and H_2) more or less uniformly. All the fluxes are raised proportionately. But in concert with higher O escape, the higher UV flux actually stabilizes CO_2 against conversion to CO, when compared to models run without the higher UV flux (not shown). The relative stability of CO_2 against high stellar UV emission has been remarked upon before [*Kasting et al.*, 1984; *Kasting*, 1995; *Segura et al.*, 2007] in studies that address how difficult it is to create O_2 atmospheres without oxygenic photosynthesis.

5.4. Changing CO_2: Alternative Oxygen Sinks

[51] Our nominal models assume that the chief vectors of soil oxidation are H_2O_2 and O_3. Hydrogen peroxide is

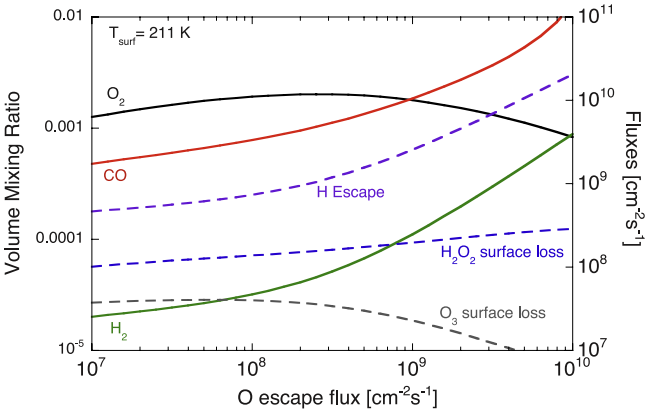

Figure 9. How the atmospheric composition and major redox fluxes change in response to changing levels of oxygen escape and solar UV flux. These are linked as described in the text.

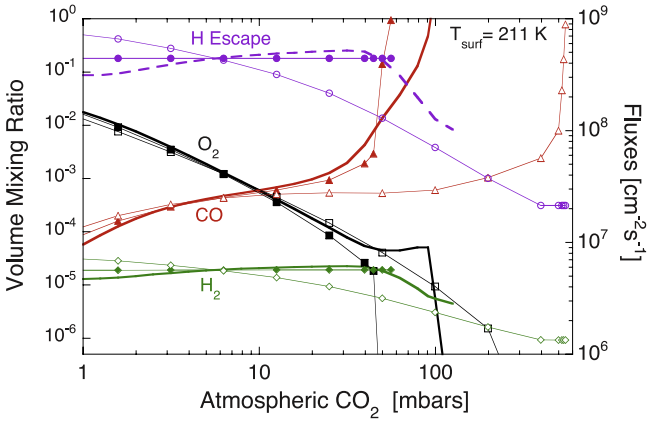

Figure 10. How different boundary conditions on oxygen change the way the atmosphere responds to changing pCO_2. The surface temperature and atmospheric water vapor are appropriate for Mars today. The bold curves refer to the nominal model in which soil is oxidized by H_2O_2 and O_3. These models become unstable at $pCO_2 \approx 100$ mbar. The open symbols denote models in which the atmospheric redox budget is balanced by O escape to space. These become unstable at $pCO_2 \approx 50$ mbar. The filled symbols denote models in which soil is oxidized by O_2, in proportion to the amount of O_2 in the atmosphere. In these models, CO_2 remains stable for $pCO_2 < 500$ mbar. There is little difference between models generated by the three different types of boundary conditions where $pCO_2 < 50$ mbar.

especially attractive because its high solubility in water makes its uptake by surface microfilms of water relatively probable; it is certainly stickier and vastly more soluble than O_2. On the other hand, O_2 is much more abundant. *Huguenin* [1973, 1976] suggested that photostimulated oxidation rates using O_2 exceed 10^8 cm^{-2} s^{-1}, comparable in order of magnitude to H escape.

[52] We implement the O_2 sink as a deposition velocity. This is not obviously a good proxy for what Huguenin suggested is happening, but it is our best choice at present. *Huguenin* [1973, 1976] showed that UV photostimulated oxidation of magnetite by O_2 gas in the presence of trace amounts of water can occur quickly. The difficulty in relating reactions that take place over tens of minutes on clean magnetite in the lab, to reactions that take place over tens of thousands of years in dirt on Mars, suggests that it would be unwise to apply Huguenin's rate constants as given. The model is tuned by adjusting v_{dep} to give a good overall fit to O_2, CO, and H_2. The best fit to the current Martian atmosphere uses $v_{dep}(O_2) = 4 \times 10^{-7}$ cm s^{-1}. The computed abundances in the tuned model are essentially identical to what we compute using H_2O_2 as the chief oxidant. This can be seen in Figure 10 at $pCO_2 = 6.3$ mbar. But when the O_2 boundary condition is applied to models with more CO_2, the decreasing O_2 provides a strong stabilizing feedback that reduces H escape and limits the growth of CO. The relative stability of these atmosphere at high pCO_2 is illustrated in Figure 10.

[53] We can also consider O escape. Models of this sort are quite likely to be relevant to early Mars because O escape rates are expected to have been very high [*Lammer et al.*, 2003]. There is no stabilizing feedback between pCO_2 and O escape while CO_2 is the major atmospheric constituent, and consequently these atmospheres are less photochemically stable than our nominal model. Results of running the model in O escape mode are also illustrated in Figure 10. Regardless of the surface sink, O escape to space suggests that cold thick CO_2 atmospheres would not have been photochemically stable on early Mars.

6. Photochemical Stability of CO_2 Atmospheres

[54] The possible photochemical instability of CO_2 atmospheres is not a new topic. It was widely discussed early in the space age, both for Mars and Venus [*McElroy and Hunten*, 1970; *McElroy*, 1972; *McElroy and Donahue*, 1972]. The matter was seen to be puzzling because CO_2 is readily photodissociated, and the direct three-body recombination, CO + O + M → CO_2+ M, is spin-forbidden and therefore extremely slow at atmospheric temperatures. The solution for Mars is that photolysis of water vapor produces OH radicals that react readily with CO to make CO_2; in effect water vapor photolysis catalyses the recombination of CO_2 [*McElroy and Donahue*, 1972]. Figures 7, 8, and 10 raise the question of the stability of CO_2 once again.

[55] Figure 11 maps out the range of photochemically stable CO_2 atmospheres in our nominal models, in which soil oxidation is by H_2O_2 and O_3 at a fixed deposition velocity of 0.02 cm s^{-1}. These models scale the eddy diffusion coefficient inversely with the square root of atmospheric density, and impose temperature structures featuring a 1.4 K km^{-1} temperature gradient extending

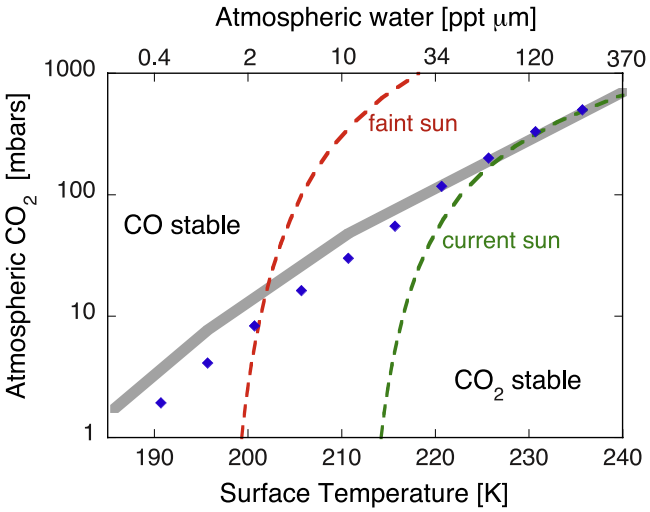

Figure 11. The photochemical stability of CO_2. CO_2 is photochemically stable against conversion to CO below and to the right of the thick gray line (modern UV and negligible oxygen escape), or below and to the right of the blue diamonds (enhanced UV and high levels of O escape, conditions suitable to 4 Ga). The two dashed curves relate surface temperature to pCO_2 according to *Kasting*'s [1991] greenhouse warming models for early (faint Sun, $0.75L_\odot$) and current Mars. It is notable that thick, cold (i.e., dry) CO_2 atmospheres would not have been photochemically stable on early Mars.

from the surface upward to a 140 K isothermal upper atmosphere. We do not attempt to self-consistently compute the radiative-convective temperature structure of the atmosphere. The relative humidity is unchanged from our base model. Model C in Table 4 provides an exemplary computation of what today's 6.3 mbar CO_2 atmosphere might have looked like 3.5 Ga.

[56] Figure 11 shows two cases, one with modern UV irradiation and negligible oxygen escape, and the other with high rates of O escape (10^9 cm^{-2} s^{-1}) and enhanced UV (factor of 10 at Lyα and a factor of 4 at $\sim$200 nm) that might be expected for Mars at circa 4 Ga. The boundary lines are for atmospheres in which the CO and CO_2 mixing ratios are equal. It turns out, somewhat surprisingly, that the more aggressive high UV, high O escape models do not impact CO_2 stability very much. Oxygen escape makes thin CO_2 atmospheres somewhat less stable against conversion to CO, but CO_2 photochemical stability on early Mars is debatable even without high rates of O escape.

[57] Figure 11 suggests that CO_2 becomes photochemically unstable in thick, dry, cold atmospheres. At low surface temperatures, appropriate to a thin atmosphere and the faint young sun, CO_2 can be unstable at surface pressures no higher than today. To put the photochemical instability boundary in context we show for comparison the relation between surface temperature and pCO_2 according to *Kasting*'s [1991] greenhouse warming models for early (faint Sun, $0.75L_\odot$) and current Mars.

[58] The apparent photochemical instability of cold CO_2 atmospheres is an interesting result, although what it means in practice is not exactly clear. First, it takes 10^7 years for an oxygen escape flux of 10^9 cm^{-2} s^{-1} to convert a 10 mbar CO_2 atmosphere to CO. It takes ten times longer to do the same to 100 mbar of CO_2. Thus, CO_2 can be unstable yet persistent.

[59] Second, we have neglected CO surface deposition specifically and CO heterogenous chemistry more generally. It is reasonable to suspect that CO, if abundant, would interact with Fe, for which it has a strong affinity, at the surface or in airborne dust, and it is reasonable to suspect that Fe at the surface or in dust might catalyze oxidation of CO by O_2 [*Huguenin*, 1976], or by H_2O_2 and O_3 that are being generated photochemically in the atmosphere. Such reactions would recombine CO_2. However, such reactions do not appear to be important today. The chief failing of purely gas-phase photochemical models is that they do not produce enough CO. Major heterogenous sinks on CO would just exacerbate the problem. Indeed most speculation of this topic [*Atreya and Gu*, 1994; *Krasnopolsky*, 1995, 2006] has gone in the other direction, suggesting that dust acts preferentially as a sink on the reactive products of H_2O photolysis, thus reducing the catalytic recombination of CO_2, and thereby increasing CO. Still, heterogenous reactions of CO might become important if CO were hundreds or thousands of times more abundant than it is now.

[60] But if we accept our results at face value, we note that the intersection of the faint sun greenhouse curve and the high O-escape CO_2 stability curve at $\sim$10 mbar and $\sim$200 K gives a valid equilibrium balance between photochemistry and the greenhouse effect. This is a stable solution because CO is a weaker greenhouse gas than CO_2. Of course, other factors, such as CO_2 condensation, are likely to be important.

7. Discussion

[61] In the early 1970s the discussion of CO_2 stability on Mars centered on the kinetic inhibition against CO_2 recombination. This is part of the matter here, but not all of it. What drives the instability seen in Figures 7 and 8 is the redox budget of the atmosphere. In these models CO builds up because the atmosphere loses O (through the surface sink and through escape to space) faster than it loses H to space. When CO becomes abundant, gas-phase chemical reactions involving CO have little further effect on O loss or H escape: all gas-phase channels are saturated, so that CO has to rise enormously to have any additional effect on the redox budget. Surface-catalyzed reactions between CO and peroxides to make CO_2, which we have not included, are likely to provide an important stabilizing feedback when CO is abundant.

[62] Active volcanoes and meteorite impacts, which we have not included in these simulations, accentuate the imbalance and speed the growth of CO. Indeed, both mechanisms have been addressed in exactly this context in earlier work. *Kasting et al.* [1982] and *Kasting* [1990] addressed the question of CO_2 instability on the context of ancient Earth. In the work by *Kasting et al.* [1982], CO runaways were triggered by too much volcanic H_2 and CH_4. These simulations implicitly invoked a strongly reduced early mantle, because the volcanic input needed to trigger a CO runaway was rather large. In the work by *Kasting* [1990], CO runaways were triggered by infall of reduced meteoritic materials during the late bombardment before 3.8 Ga when impact rates were high. The reduced material in the meteorites, in particular metallic Fe (which is abundant in many classes of meteorites), reacted with atmospheric CO_2 at high temperatures to make CO and FeO. Thus the atmosphere became more reduced, and CO built up. Although *Kasting* [1990] used higher impact rates before 4.2 Ga than we would use today, the arguments made and conclusions reached in that study are qualitatively correct and, if anything, more powerfully applied to the cold dry climate of ancient Mars than to the warm wet climate of early Earth.

[63] An interesting point is that the stability question is asymmetric. Under plausible conditions a significant CO atmosphere can be converted to a CO_2 atmosphere quickly, because the driver for oxidation is hydrogen escape, which can be fast, and the driver for recombination is water vapor, which can become very abundant very quickly if the right sort of event takes place (e.g., a major impact or a volcanic flood). As a specific example, if the atmosphere were hydrogen-rich or water-rich, diffusion-limited hydrogen escape rates can approach 10^{13} cm^{-2} s^{-1}, which is fast enough to transform a 100 mbar CO atmosphere into a CO_2 atmosphere in as little as 10^4 years. These points taken together suggest that hysteresis is likely: transient warm wet epochs can quickly establish CO_2 atmospheres that only slowly decay to CO in the long years after the warmth and the wet have gone away.

[64] Abundant CO might produce strong subsurface redox gradients, if oxidants are concentrated at the surface and

CO permeates the deeper soils. A speculative possibility is that abundant CO might favor the formation of metal carbonyls. These are volatile substances that can provide a nontraditional means of mobilizing certain metals, particularly in locally reduced settings. Nickel and iron are the best known carbonyls; $Ni(CO)_4$ is the most stable, the most volatile, and the most interesting. Metal carbonyls give us some hope that an ancient CO-rich atmosphere of Mars might have left behind some distinctive observable consequences. It is interesting that high Ni abundances have been reported by MER in Gusev soils [*Yen et al.*, 2005, 2006]. The excess Ni has been interpreted as meteoritic contamination, and its evident mobility (it is enriched in hematite spherules) has been interpreted as transport by a chloride-rich brine [*Yen et al.*, 2006]. These are plausible hypotheses; indeed a meteoritic source seems almost unassailable in the absence of alchemy. But the geochemical mobility of nickel at the Martian surface might also be explained by mobilization of nickel as a carbonyl, especially if the observed anomalies lie mostly with nickel, as *Yen et al.* [2005, 2006] suggest. Indeed iron-nickel meteorites would seem a perfect substrate for making carbonyls.

8. Conclusions

[65] We develop a new 1-D gas phase photochemical model of the Martian atmosphere that gives generally good agreement with the observed mixing ratios of the important photochemical product gases O_2, CO, and H_2. Our model, especially model B with a dry stratosphere (Table 4), does a good job predicting the abundances of O_2, CO, H_2O_2, and H_2.

[66] One difference between our model and other 1D photochemical models is that we have assumed that the atmosphere's redox budget is balanced by a surface sink on reactive oxidized gases, chiefly H_2O_2 and O_3, that we have implemented as a deposition velocity. Our choice of a surface sink for oxygen, as opposed to O escape to space, is driven by the observational and theoretical consensus that O escape to space is currently negligible [*Lammer et al.*, 2003]. The surface oxygen sink requires that hydrogen peroxide and ozone react with ferrous iron and sulfides; we do not address how this happens, although it is known that if water is temporarily present, alkaline earth and alkali hydroxides can form [*Oyama and Berdahl*, 1979], so it has been suggested that even in cold environments, thin films of water may have been important on Mars [*Yen et al.*, 2005]. Mass balance suggests that the wave of oxidation penetrates the Martian crust at a rate of order of 10 m Ga^{-1}, less if sulfides are abundant.

[67] The other major difference between our model and other models is that we have accepted diffusion-limited hydrogen escape. The observed hydrogen escape flux is the least compelling of the constraints traditionally applied to photochemical models. One reason is that the escape flux is not directly measured: it is inferred from the observed number densities as fit to a model. Another reason is that the arguments in favor of diffusion-limited H escape from Mars are strong: (1) The assumption of a Maxwellian velocity distribution function used by *Anderson and Hord* [1971] predicts exospheric H densities and escape fluxes that are about half what more accurate velocity distribution functions predict [*Galli et al.*, 2006b; *Cui et al.*, 2008; *Barakat and Schunk*, 2007]. (2) The estimated escape fluxes using *Galli et al.*'s [2006a, 2006b] models are essentially identical to the diffusion-limited flux one obtains using *Krasnopolsky and Feldman*'s [2001] measurement of 17 ppmv H_2 in the lower atmosphere. (3) Escape fluxes inferred from *Galli et al.*'s [2006a, 2006b] models are the same when the exobase temperature is 350 K, 425 K, and 1000 K; this implies that the bottleneck to escape is established at a lower altitude. (4) Our photochemical model predicts that the H_2 mixing ratio should be $\sim$20 ppmv if and only if escape is at the diffusion limit; by contrast the same model tuned to give the lower Anderson and Hord escape flux predicts H_2 volume mixing ratios of 40–50 ppmv. These four arguments in favor of diffusion-limited flux are logically independent; that they converge on the same point is noteworthy.

[68] We then apply our model to Martian atmospheres that differ somewhat from today's atmosphere. We include O escape for ancient Mars. We find that cold CO_2 atmospheres can be photochemically unstable, especially on early Mars when the faint Sun encourages colder climates. For ancient Mars, CO_2 stability would be further compromised by other sources of reducing power (active volcanism, a more reduced crust, and substantial exogenous input of reduced meteoritic iron during the late bombardment) that are not important today.

[69] Our results challenge the common assumption that early Mars was wrapped in a thick CO_2 atmosphere. On the other hand it takes a long time to reduce a CO_2 atmosphere to CO. We estimate that it could take as long as 10^8 years to reduce a photochemically unstable 100 mbar CO_2 atmosphere to CO, if an oxygen escape flux of 10^9 cm^{-2} s^{-1} is indicative of the order of magnitude of the forcing. This is the same order of magnitude of forcing as modern terrestrial volcanism. Of course, the timescales would be shorter if volcanoes were more active, or reduced iron in impacts important, or if ferrous or sulfidic minerals were stronger sinks of oxidized gases or acids than today, or the O escape were faster; nonetheless the timescales for evolving the atmosphere were probably long enough that steady state solutions should be regarded as goals rather than as achievements. CO_2 atmospheres can be unstable but persistent simply because there isn't time enough to destroy them.

[70] Finally, it is worth pointing out that a lot of CO in an atmosphere is not just an inconvenience. For life it is an opportunity. The possible role of CO in the origin of life has been mooted many times, usually but not exclusively in the context of metabolism-first scenarios. CO is packed with energy. Methanogenesis takes CO and hydrogenates it with a catalyst based on iron-nickel sulfides; carboxydotrophy takes CO and oxidizes it with a catalyst based on iron-nickel sulfides [*Ragsdale*, 2004]. These are ancient metabolisms. The possibility that metabolism began with CO and an Fe- or Ni-based catalyst is quite reasonable, as *Ragsdale* [2004] notes in his review. A CO-rich early atmosphere may well make a cold young Mars seem a more attractive place to look for the first steps toward life.

[71] **Acknowledgments.** We thank Mark Claire, Pat Hamill, and Robert Chatfield for helpful improvements of the photochemical code. We also thank Darrell Strobel, Bob Johnson, Roger Yelle, and Jun Cui for

discussions, insightful comments, and prepublication manuscripts addressing problems related to diffusion-limited escape. We thank NASA's Exobiology Program, Planetary Atmospheres Program, and the Mars Fundamental Research Program for support. D.C. also acknowledges the support of an EU Marie Curie Chair.

References

Anderson, D. E. (1974), Mariner 6, 7, and 9 ultraviolet spectrometer experiment: analysis of hydrogen Lyman-alpha data, *J. Geophys. Res.*, *79*, 1513–1518.

Anderson, D. E., and C. W. Hord (1971), Mariner 6 and 7 ultraviolet spectrometer experiment: Analysis of hydrogen Lyman-alpha data, *J. Geophys. Res.*, *76*, 6666–6673.

Atkinson, R., D. L. Baulch, R. A. Cox, R. F. Hampson Jr., J. A. Kerr, and J. Troe (1989), Evaluated kinetic and photochemical data for atmospheric chemistry: Supplement III, *J. Phys. Chem. Ref. Data*, *18*, 881–1097.

Atkinson, R., D. L. Baulch, R. A. Cox, J. N. Crowley, R. F. Hampson, R. G. Hynes, M. E. Jenkin, M. J. Rossi, and J. Troe (2004), Evaluated kinetic and photochemical data for atmospheric chemistry: Volume I - Gas phase reactions of O_x, HO_x, NO_x and SO_x species, *Atmos. Chem. Phys.*, *4*, 1461–1738.

Atreya, S. K., and Z. G. Gu (1994), Stability of the Martian atmosphere: Is heterogeneous catalysis essential?, *J. Geophys. Res.*, *99*, 13,133–13,145.

Barakat, A. R., and R. W. Schunk (2007), Monte Carlo vs. transport equations' description of outflowing fully-ionized ionospheric plasma, *Eos Trans. AGU*, *88*(52), Fall Meet. Suppl., Abstract SA51B-0522.

Barakat, A. R., I. A. Berghouti, and R. W. Schunk (1995), Double-hump H+ velocity distribution in the polar wind, *Geophys. Res. Lett.*, *22*, 1857–1860.

Baulch, D. L., C. J. Cobos, R. A. Cox, C. Esser, P. Frank, T. Just, J. A. Kerr, M. J. Pilling, J. Troe, R. W. Walker, and J. Warnatz (1992), Evaluated kinetic data for combustion modelling, *J. Phys. Chem. Ref. Data*, *21*, 411–429.

Baulch, D. L., et al. (1994), Evaluated kinetic data for combustion modelling, supplement I, *J. Phys. Chem. Ref. Data*, *23*, 847–1043.

Biemann, K., et al. (1977), The search for organic substances and inorganic volatile compounds in the surface of Mars, *J. Geophys. Res.*, *82*, 4641–4658.

Bullock, M. A., C. R. Soker, C. P. McJay, and A. P. Zent (1994), A coupled soil-atmosphere model of H_2O_2 on Mars, *Icarus*, *107*, 142–154.

Chyba, C. F., S. W. Squyres, and C. Sagan (1989), Depth to unoxidized material in the Martian regolith, *Lunar Planet. Sci. Conf.*, *XX*, 157–158.

Claire, M. W., D. C. Catling, and K. J. Zahnle (2006), Biogeochemical modeling of the rise in atmospheric oxygen, *Geobiology*, *4*, 239–269.

Cui, J., R. Yelle, and K. Volk (2008), Distribution and escape of molecular hydrogen in Titan's thermosphere and exosphere, *J. Geophys. Res.*, *113*, E10004, doi:10.1029/2007JE003032.

Davidson, J. A., H. I. Schiff, T. J. Brown, and C. J. Howard (1978), Temperature dependence of the deactivation of $O(^1D)$ by CO from 113–333 K, *J. Chem. Phys.*, *69*, 1216–1217.

Donahue, T. M., D. H. Grinspoon, R. E. Hartle, and R. R. Hodges (1997), Ion/neutral escape of hydrogen and deuterium: Evolution of water, in *Venus II*, edited by S. W. Bougher, D. M. Hunten, and R. J. Phillips, pp. 385–414, Univ. of Ariz. Press, Tucson.

Farquhar, J., J. Savarino, T. L. Jackson, and M. H. Thiemans (2000), Evidence of atmospheric sulfur in the Martian regolith from sulphur isotopes in meteorites, *Nature*, *404*, 50–52.

Farquhar, J., S.-T. Kim, and A. Masterson (2007), Implications from sulfur isotopes of the Nakhla meteorite for the origin of sulfate on Mars, *Earth Planet. Sci. Lett.*, *264*, 1–8, doi:10.1016/j.epsl.2007.08.006.

Forget, F., and R. T. Pierrehumbert (1997), Warming early Mars with carbon dioxide clouds that scatter infrared radiation, *Science*, *278*, 1273–1276.

Fox, J., and A. Hac (1997), Spectrum of hot O at the exobases of the terrestrial planets, *J. Geophys. Res.*, *102*, 24,005–24,011.

Friedrichs, G., J. T. Herbon, D. F. Davidson, and R. K. Hanson (2002), Quantitative detection of HCO behind shock waves: The thermal decomposition of HCO, *Phys. Chem. Chem. Phys.*, *4*, 5778–5788.

Galli, A., P. Wurz, S. Barabash, A. Grigoriev, H. Gunell, R. Lundin, M. Holmström, and A. Fedorov (2006a), Energetic Hydrogen and Oxygen Atoms Observed on the nightside of Mars, *Space Sci. Rev.*, *126*, 267–297.

Galli, A., P. Wurz, H. Lammer, H. I. M. Lichtenegger, R. Lundin, S. Barabash, A. Grigoriev, M. Holmström, and H. Gunell (2006b), The hydrogen exospheric density profile measured with ASPERA-3/NPD, *Space Sci. Rev.*, *126*, 447–467.

Haberle, R. M. (1998), Early Mars climate models, *J. Geophys. Res.*, *103*, 28,467–28,480.

Hoefen, T. M., R. N. Clark, J. L. Bandfield, M. D. Smith, J. C. Pearl, and P. R. Christensen (2003), Discovery of olivine in the Nili Fossae region of Mars, *Science*, *302*, 627–630.

Huguenin, R. L. (1973), Photostimulated oxidation of magnetite, *J. Geophys. Res.*, *78*, 8481–8506.

Huguenin, R. L. (1976), Mars—Chemical weathering as a massive volatile sink, *Icarus*, *28*, 203–213.

Hunten, D. M. (1974), The escape of light gases from planetary atmospheres, *J. Atmos. Sci.*, *30*, 1481–1494.

Hunten, D. M. (1979), Possible oxidant sources in the atmosphere and surface of Mars, *J. Mol. Evol.*, *14*, 57–64.

Hunten, D. M. (1990), Kuiper prize lecture: Escape of atmospheres, ancient and modern, *Icarus*, *85*, 1–20.

Inn, E. C. Y. (1974), Rate of recombination of oxygen atoms and CO at temperatures below ambient, *J. Chem. Phys.*, *61*, 1589–1594.

Inomata, S., and N. Washida (1999), Rate constants for the reactions of NH_2 and HNO with atomic oxygen at temperatures between 242 and 473 K, *J. Phys. Chem. A*, *103*, 5023–5031.

Jeans, J. H. (1925), *The Dynamical Theory of Gases*, Cambridge Univ. Press, Cambridge, U. K.

Kasting, J. F. (1990), Bolide impacts and the oxidation state of carbon in the Earth's early atmosphere, *Origins Life*, *20*, 199–231.

Kasting, J. F. (1991), CO_2 condensation and the climate of early Mars, *Icarus*, *94*, 1–13.

Kasting, J. F. (1995), O_2 concentrations in dense primitive atmospheres: Commentary, *Planet. Space Sci.*, *43*, 11–13.

Kasting, J. F., and L. L. Brown (1998), Setting the stage: The early atmosphere as a source of biogenic compounds, in *The Molecular Origins of Life: Assembling the Pieces of the Puzzle*, edited by A. Brack, pp. 35–56, Cambridge Univ. Press, Cambridge, U. K.

Kasting, J. F., K. Zahnle, and J. C. G. Walker (1982), Photochemistry of methane in the Earth's early atmosphere, *Precambrian Res.*, *20*, 121–148.

Kasting, J. F., J. B. Pollack, and D. Crisp (1984), Effects of high CO_2 levels on surface temperature and atmospheric oxidation state on the early Earth, *J. Atmos. Chem.*, *1*, 403–428.

Kasting, J. F., K. J. Zahnle, J. P. Pinto, and A. T. Young (1989), Sulfur, ultraviolet radiation, and the early evolution of life, *Origins Life*, *19*, 95–108.

Klein, H. P. (1977), The Viking biological investigation: General aspects, *J. Geophys. Res.*, *82*, 4677–4680.

Klingelhofer, G., R. V. Morris, P. A. De Souza, D. Rodionov, and C. Schroder (2006), Two Earth years of Mossbauer studies of the surface of Mars with MIMOS II, *Hyperfine Interact.*, *170*, 169–177.

Krasnopolsky, V. A. (1993), Photochemistry of the Martian atmosphere (mean conditions), *Icarus*, *101*, 313–332.

Krasnopolsky, V. A. (1995), Uniqueness of a solution of a steady state photochemical problem: Applications to Mars, *J. Geophys. Res.*, *100*, 3263–3276.

Krasnopolsky, V. A. (2006), Photochemistry of the Martian atmosphere: Seasonal, latitudinal, and diurnal variations, *Icarus*, *185*, 153–170.

Krasnopolsky, V. A., and P. D. Feldman (2001), Detection of molecular hydrogen in the atmosphere of Mars, *Science*, *294*, 1914–1917.

Lammer, H., H. I. M. Lichtenegger, C. Kolb, I. Ribas, E. F. Guinan, R. Abart, and S. J. Bauer (2003), Loss of water from Mars: Implications for the oxidation of the soil, *Icarus*, *165*, 9–25.

Lichtenegger, H. I. M., H. Lammer, Y. N. Kulikov, S. Kazeminejad, G. H. Molina-Cuberos, R. Rodrigo, B. Kazeminejad, and G. Kirchengas (2006), Effects of low energetic neutral atoms on Martian and Venusian dayside exospheric temperature estimations, *Space Sci. Rev.*, *126*, 468–501.

Liu, S. C., and T. M. Donahue (1976), The regulation of hydrogen and oxygen escape from Mars, *Icarus*, *28*, 231–246.

Luhmann, J. G. (1997), Correction to "The ancient oxygen exosphere of Mars: Implications for atmosphere evolution" by Zhang et al., *J. Geophys. Res.*, *102*, 1637–1638.

Luhmann, J. G., R. E. Johnson, and M. G. H. Zhang (1992), Evolutionary impact of sputtering of the Martian atmosphere by O^+ pick up ions, *Geophys. Res. Lett.*, *19*, 2151–2154.

Manning, C. V., C. P. McKayb, and K. J. Zahnle (2006), Thick and thin models of the evolution of carbon dioxide on Mars, *Icarus*, *180*, 38–59, doi:10.1016/j.icarus.2005.08.014.

Marrero, T. R., and E. A. Mason (1972), Gaseous diffusion coefficients, *J. Phys. Chem. Ref. Data*, *1*, 3–118.

McElroy, M. B. (1972), Mars: An evolving atmosphere, *Science*, *175*, 443–445, doi:10.1126/science.175.4020.443.

McElroy, M. B., and T. M. Donahue (1972), Stability of the Martian atmosphere, *Science*, *177*, 986–988.

McElroy, M. B., and D. M. Hunten (1970), Photochemistry of CO_2 in the atmosphere of Mars, *J. Geophys. Res.*, *75*, 1188–1201.

McElroy, M. B., and T. Y. Kong (1976), Oxidation of the Martian surface: Constraints due to chemical processes in the atmosphere, *Geophys. Res. Lett.*, *3*, 569–572.

McElroy, M. B., T. Y. Kong, and Y. L. Yung (1977), Photochemistry and evolution of Mars's atmosphere; A Viking perspective, *J. Geophys. Res.*, *82*, 4379–4388.

McSween, H. Y., et al. (2006), Characterization and petrologic interpretation of olivine-rich basalts at Gusev Crater, Mars, *J. Geophys. Res.*, *111*, E02S10, doi:10.1029/2005JE002477.

Morris, R. V., et al. (2006), Mössbauer mineralogy of rock, soil, and dust at Gusev crater, Mars: Spirit's journey through weakly altered olivine basalt on the plains and pervasively altered basalt in the Columbia Hills, *J. Geophys. Res.*, *111*, E02S13, doi:10.1029/2005JE002584.

Mustard, J. F., F. Poulet, A. Gendrin, J. P. Bibring, Y. Langevin, B. Gondet, N. Mangold, G. Bellucci, and F. Altieri (2005), Olivine and pyroxene diversity in the crust of Mars, *Science*, *307*, 1594–1597.

Nair, H., M. Allen, A. D. Anbar, Y. L. Yung, and R. T. Clancy (1994), A photochemical model of the Martian atmosphere, *Icarus*, *111*, 124–150.

Nakamura, T., and E. Tajika (2003), Climate change of Mars-like planets due to obliquity variations: implications for Mars, *Geophys. Res. Lett.*, *30*(13), 1685, doi:10.1029/2002GL016725.

Nesbitt, F. L., J. F. Gleason, and L. J. Stief (1989), Temperature dependence of the rate constant for the reaction HCO + O_2 → HO_2 + CO at T = 200–398 K, *J. Phys. Chem. A*, *103*, 3038–3043.

Oyama, V. I., and B. J. Berdahl (1979), A model of Martian surface chemistry, *J. Mol. Evol.*, *14*, 199–210.

Pollack, J. B., J. F. Kasting, S. M. Richardson, and K. Poliakoff (1987), The case for a wet, warm climate on early Mars, *Icarus*, *71*, 203–224.

Ragsdale, S. W. (2004), Life with carbon monoxide, *Crit. Rev. Biochem. Mol. Biol.*, *39*, 165–195.

Robie, D. C., S. Arepalli, N. Presser, T. Kitsopoulos, and R. J. Gordon (1990), The intramolecular kinetic isotope effect for the reaction O(^{3}P)+HD, *J. Chem. Phys.*, *92*, 7382–7392.

Sander, S. P., et al. (2003), Chemical kinetics and photochemical data for use in atmospheric studies, evaluation number 14, *JPL Publ. 02_25*.

Schunk, R. W. (1975), Transport equations for aeronomy, *Planet. Space Sci.*, *23*, 437–485.

Seinfeld, J. W., and S. Pandis (2006), *Atmospheric Chemistry and Physics: From Air Pollution to Climate Change*, 2nd ed., 1232 pp., Wiley-Interscience, New York.

Segura, A., V. S. Meadows, J. F. Kasting, D. Crisp, and M. Cohen (2007), Abiotic formation of O_2 and O_3 in high-CO_2 terrestrial atmospheres, *Astron. Astrophys.*, *472*, 665–679.

Squyres, S., and A. Knoll (2005), Sedimentary rocks at Meridiani Planum: Origin, diagenesis, and implications for life on Mars, *Earth Planet. Sci. Lett.*, *240*, 1–10, doi:10.1016/j.epsl.2005.09.038.

Sun, F., J. D. DeSain, G. Scott, P. Y. Hung, R. I. Thompson, G. P. Glass, and R. F. Curl (2001), Reactions of NH_2 with NO_2 and of OH with NH_2O, *J. Phys. Chem. A*, *105*, 6121–6128.

Toon, O. B., J. B. Pollack, W. Ward, J. A. Burns, and K. Bilski (1980), The astronomical theory of climatic change on Mars, *Icarus*, *44*, 552–607.

Tsang, W., and J. T. Herron (1991), Chemical kinetic data base for propellant combustion. I. Reactions involving NO, NO_2, HNO, HNO_2, HCN and N_2O, *J. Phys. Chem. Ref. Data*, *20*, 609–663.

Wagner, A. F., and J. M. Bowman (1987), The addition and dissociation reaction H + CO → HCO. 1. Theoretical RRKM studies, *J. Phys. Chem.*, *91*, 5314–5324.

Walker, J. C. G. (1977), *Evolution of the Atmosphere*, Macmillan, New York.

Wong, A., S. K. Atreya, and T. Encrenaz (2003), Chemical markers of possible hot spots on Mars, *J. Geophys. Res.*, *108*(E4), 5026, doi:10.1029/2002JE002003. (Correction to "Chemical markers of possible hot spots on Mars," *J. Geophys. Res.*, *109*, E01007, doi:10.1029/2003JE002210, 2004.)

Yen, A. S., et al. (2005), An integrated view of the chemistry and mineralogy of Martian soils, *Nature*, *436*, 49–54.

Yen, A. S., et al. (2006), Nickel on Mars: Constraints on meteoritic material at the surface, *J. Geophys. Res.*, *111*, E12S11, doi:10.1029/2006JE002797.

Yung, Y., and W. B. DeMore (1998), *The Photochemistry of Planetary Atmospheres*, 480 pp., Oxford Univ. Press, New York.

Zahnle, K. J., J. F. Kasting, and J. B. Polack (1990), Mass fractionation of noble gases in diffusion-limited hydrodynamic hydrogen escape, *Icarus*, *84*, 503–527.

Zahnle, K. J., M. W. Claire, and D. C. Catling (2006), The loss of mass-independent fractionation in sulfur due to a Paleoproterozoic collapse of atmospheric methane, *Geobiology*, *4*, 271–282.

Zent, A. P. (1998), On the thickness of the oxidized layer of the Martian regolith, *J. Geophys. Res.*, *103*, 31,491–31,498.

D. C. Catling, Department of Earth Sciences, University of Bristol, Wills Memorial Building, Bristol BS8 1RJ, UK.

R. M. Haberle and K. Zahnle, NASA Ames Research Center, MS 245-3, Moffett Field, CA 94035, USA. (kzahnle@mail.arc.nasa.gov)

J. F. Kasting, Department of Geosciences, Pennsylvania State University, 443 Deike Building, State College, PA 16802, USA.